iScience

Article

M-Motif, a potential non-conventional NLS in YAP/TAZ and other cellular and viral proteins that inhibits classic protein import

Graphical abstract

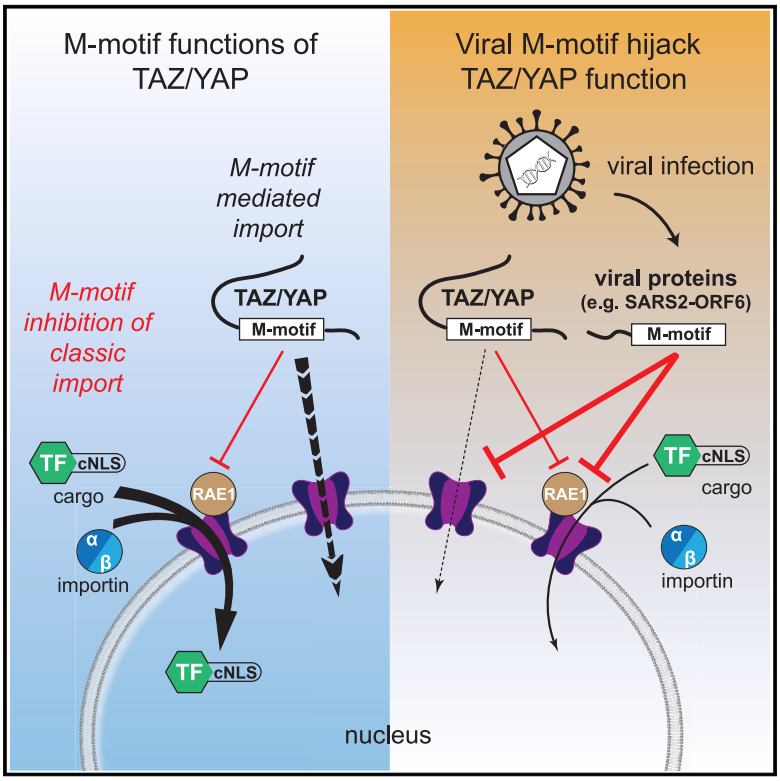

Highlights

- TAZ/YAP contain a non-conventional NLS, the M-motif, mediating Ran-independent import
- The M-motif harbors an obligate methionine (M) flanked by negative charges
- Several cellular and viral proteins possess import-competent M-motifs
- TAZ via its M-motif inhibits classic nuclear import, a feature hijacked by viruses

Authors

Michael Kofler, Shruthi Venugopal, Gary Gill, Caterina Di Ciano-Oliveira, András Kapus

Correspondence

michael.kofler@unityhealth.to (M.K.), andras.kapus@unityhealth.to (A.K.)

In brief

Molecular Structure; Molecular interaction; Cell biology

Kofler et al., 2025, iScience *28*, 112105
April 18, 2025
https://doi.org/10.1016/j.isci.2025.112105

CellPress

iScience

CellPress
OPEN ACCESS

Article

M-Motif, a potential non-conventional NLS in YAP/TAZ and other cellular and viral proteins that inhibits classic protein import

Michael Kofler,[1,*] Shruthi Venugopal,[1] Gary Gill,[1] Caterina Di Ciano-Oliveira,[1] and András Kapus[1,2,3,4,*]
[1]Keenan Research Centre for Biomedical Science of the St. Michael's Hospital, Toronto, ON, Canada
[2]Department Surgery, University of Toronto, Toronto, ON M5B 1T8, Canada
[3]Department Biochemistry, University of Toronto, Toronto, ON M5B 1T8, Canada
[4]Lead contact
*Correspondence: michael.kofler@unityhealth.to (M.K.), andras.kapus@unityhealth.to (A.K.)
https://doi.org/10.1016/j.isci.2025.112105

SUMMARY

Multiple mechanisms were proposed to mediate the nuclear import of TAZ/YAP, transcriptional co-activators regulating organ growth and regeneration. Our earlier observations showed that TAZ/YAP harbor a C-terminal, unconventional nuclear localization signal (NLS). Here, we show that this sequence, necessary and sufficient for basal, ATP-independent nuclear import, contains an indispensable central methionine flanked by negatively charged residues. Based on these features, we define the M-motif and propose that it is a new class of NLS, also present and import-competent in other cellular (STAT1 and cyclin B1) and viral (ORF6 of SARS-CoV2, VSV-M) proteins. Accordingly, ORF6 SARS-Cov2 competitively inhibits TAZ/YAP uptake, while TAZ abrogates STAT1 import. Similar to viral M-motif proteins, TAZ binds RAE1 and inhibits classic nuclear protein import, including that of antiviral factors (IRF3 and NF-κB). However, RAE1 is dispensable for TAZ import itself. Thus, the TAZ/YAP NLS has a dual function: it mediates unconventional nuclear import and inhibits classic import, contributing to the suppression of antiviral responses.

INTRODUCTION

TAZ and YAP are paralogous transcriptional coactivators, impacting growth, differentiation, tissue plasticity and extracellular matrix production.[1,2] Being key regulators of development and regeneration, they also play central roles in the pathogenesis of various cancers[3–5] and organ fibrosis.[6–11] TAZ/YAP are regulated by two major – and interconnected – networks: the Hippo kinase pathway and the cytoskeleton.[12–14] These systems relay an array of environmental inputs to TAZ/YAP, including cell contact integrity, presence of extracellular ligands, metabolic state, matrix stiffness, and other mechanical cues.[15–22] The Hippo pathway and the cytoskeleton control both TAZ/YAP expression (synthesis and degradation)[23,24] and transcriptional *activity.* The latter is primarily determined by the regulation of TAZ/YAP nuclear accumulation. The vast majority of the literature interprets the control of their *localization* in the context of *retention models*. Thus, Hippo pathway-mediated phosphorylation of TAZ/YAP ensures their interaction with 14-3-3 proteins, and consequent cytosolic retention.[25,26] Similarly, actin polymerization has been shown to alter the binding of TAZ/YAP to angiomotin proteins, which also act as cytosolic retention factors.[27,28] Once liberated, TAZ/YAP enter the nucleus, where they bind to their intranuclear partners, predominantly members of the TEAD family of transcription factors.[29,30] This results in the activation of gene transcription and intranuclear retention.[31–33]

While the structural basis and regulation of compartmental retention have been worked out in detail, relatively little was known about the actual *nucleocytoplasmic shuttling* (import and export) of TAZ/YAP. Although early studies showed that their intranuclear accumulation involves certain sequence motifs, such as the C-terminal PDZ-binding motif (PBM),[34] it remained unclear whether they affect retention, import or export. Moreover, since TAZ/YAP do not contain a classic nuclear localization signal (NLS) or a typical nuclear export signal (NES), it was uncertain whether they enter and leave the nucleus by simple diffusion or by mediated transport. We were the first to address these issues.[32] Using rigorous approaches – e.g., nuclear entry of 5-Citrine-tagged TAZ fusions that are too large for passive diffusion through the nuclear pore – we have shown that both TAZ import and export are mediated processes. We have identified a C-terminal region (327–341) that worked as a bona fide NLS, which we termed "TAZ NLS" (Figure 1A). It is a highly unconventional, negatively charged import motif that appears to mediate Ran-independent import. We have also identified a CRM1-dependent NES in the TAZ N-terminus, which is masked by TEAD.

Subsequent work has given credence to the notion that TAZ/YAP might utilize multiple import mechanisms that operate under various regulatory conditions or tissue contexts (reviewed in[35]). For example, TAZ/YAP were shown to bind to mastermind-like and mask family proteins which contain a classic NLS and shuttle them into the nucleus by a piggyback mechanism.[36,37]

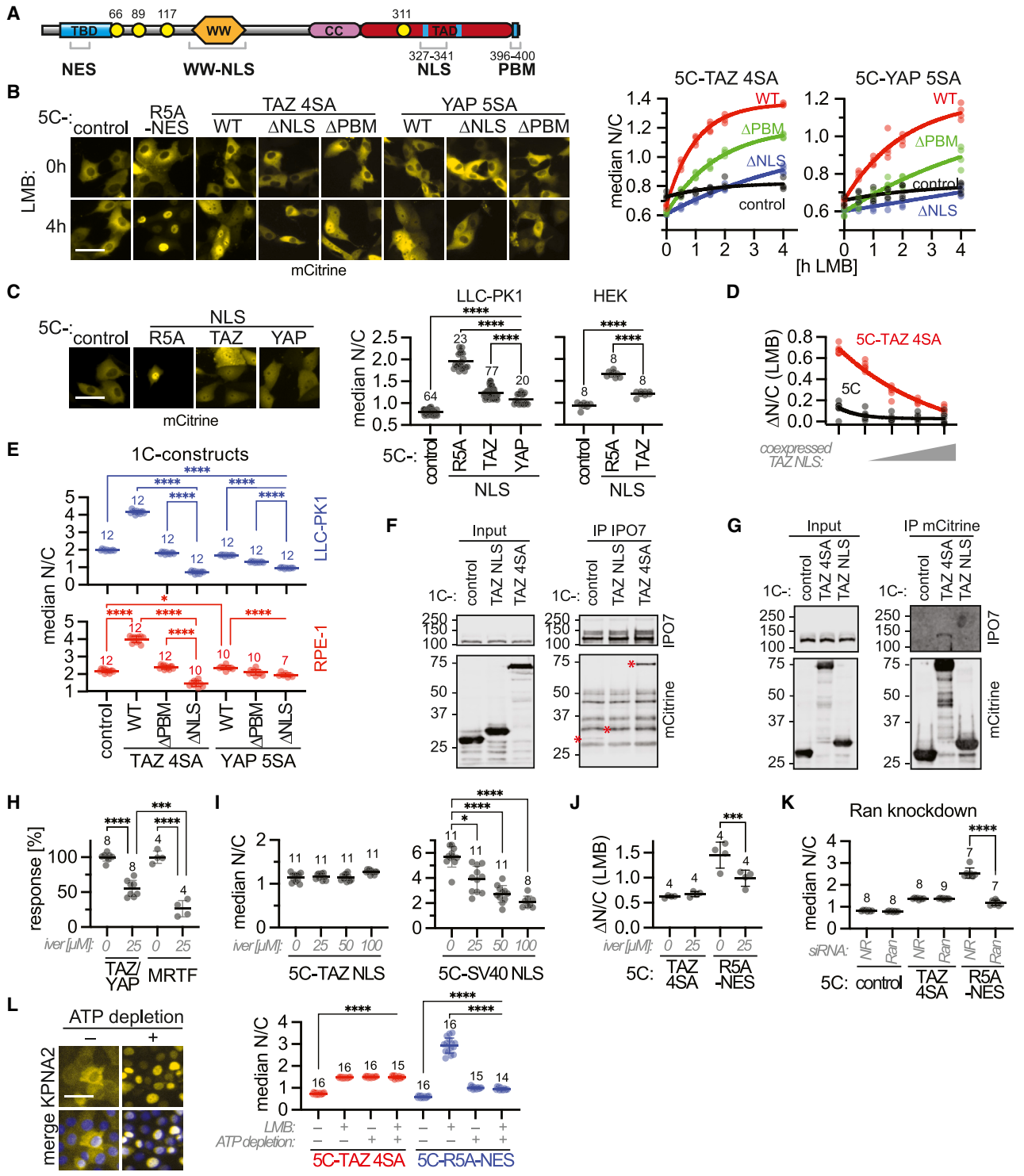

Figure 1. Characterization of structural requirements and functional properties of TAZ and YAP nuclear import

(A) Domain organization of TAZ with regions important for nucleocytoplasmic shuttling highlighted. Lats-phosphorylation sites are shown as yellow circles with labels, hydrophobic motifs FLxx[I,V,L,M] as blue lines. CC: coiled-coil region; NES: nuclear export signal; NLS: nuclear localization signal; PBM: PDZ domain binding motif; TAD: transactivation domain; TBD: TEAD-binding domain; WW: WW domain; WW-NLS: globular NLS composed of the WW domain.

(B) Localization of diffusion-limited 5C constructs in pig proximal tubular epithelial LLC-PK1 cells, also see Figure S1. 5C-R5A-NES: shuttling control comprising a variant of the SV40 NLS and the HIV Ref NES. WT: 5C-TAZ 4SA or 5C-YAP 5SA; ΔNLS: constructs with deletion of residues 321–345 (TAZ) or 413–427 (YAP); ΔPBM: constructs missing the last 5 aa (the PBM); control: 5C control. Left: Representative fluorescence microscopy images of transfected cells, without (top)

(legend continued on next page)

Further, importin-α5 was found to be important for TAZ uptake.[38] A subsequent study showed that the YAP PBM binds Importin-7 (IPO7), which can catalyze YAP nuclear uptake in the context of mechanotransduction.[39] Finally, while this work was under review, a study was published that identified the TAZ/YAP WW domain as a globular NLS[40] utilizing the classic import machinery for YAP influx. In addition to these import studies, nuclear efflux of TAZ/YAP was shown to be highly regulated.[41,42]

Despite such impressive progress in the field, fundamental questions remain open. Here, we concentrated on the C-terminal "TAZ NLS" described by us earlier. We wished to get insight into (1) the exact sequence requirements for its function, (2) its fundamental functional characteristics, and (3) its potential presence and significance in other proteins, i.e., the very definition and generalizability of this import motif as a new class of NLS.

The *first part* of this work will present evidence that negative charges flanking a central methionine are essential for the function of this import motif. These newly recognized characteristics allowed us to define the TAZ/YAP NLS, as an "M-motif", which is present and import-competent in a variety of key cellular and viral proteins. We also show that the M-motif mediates ATP-independent facilitated influx. Nonetheless, the exact molecular mechanism for the M-motif-dependent import remains to be elucidated. However, during these studies, we discovered that TAZ, via its M-motif, potently inhibits classic protein import, similar to viral M-motifs.[43–52] Accordingly, the *second part* of this study describes this phenomenon and shows that the TAZ M-motif exerts this inhibitory effect predominantly through its binding partner, the nuclear pore protein ribonucleic acid export-1 (RAE1). Importantly, TAZ/YAP inhibit the classic import of key antiviral factors (IRF3 and NF-κB), which might signify a new mechanism contributing to their suppressive effect of antiviral responses.[53–55]

RESULTS

Basic characteristics of TAZ/YAP NLS-mediated import

For the basic characterization of their import, we used Lats phosphorylation site mutants of full-length TAZ and YAP (TAZ 4SA, and YAP 5SA), to eliminate 14-3-3-mediated cytosolic retention. Proteins were fused to a five Citrine (5C) tag for visualization and to minimize nuclear influx driven by passive diffusion. We also monitored two controls (negative and positive): the 5C-tag alone and construct 5C-R5A-NES, containing a classic NLS (R5A) and an NES to ensure cycling across the nuclear membrane, as is the case with TAZ and YAP.[32] Under steady-state (resting) conditions, all constructs localized to the cytoplasm, hence having low nuclear-to-cytoplasmic fluorescence ratios (N/C) (Figure 1B). This is consistent with the fact that in the cycling constructs, the CRM1-dependent nuclear export surmounts import.[32] Addition of Leptomycin B (LMB), a potent inhibitor of CRM1-mediated export, did not change the localization of the 5C-tag, verifying the absence of diffusional or mediated uptake and indicating the intactness of the nuclear membrane. In contrast, LMB induced potent nuclear entry of 5C-R5A-NES, 5C-TAZ 4SA, and 5C-YAP 5SA (Figure 1B), confirming that TAZ and YAP access the nucleus in a mediated fashion. (Of note, the overall accumulation of 5C-R5A-NES, harboring a classic NLS was larger, see Figure S1). Next, we tested the role of the NLS: deletion of this segment from full-length TAZ and YAP constructs (ΔNLS) essentially eliminated net entry, indicating that the NLS is indispensable for mediated import of both TAZ and YAP. The isolated NLS, on the other hand, retained import competence, as evidenced by the steady state localization of the 5C-TAZ/YAP NLS constructs (Figure 1C).[32,56] Similar observations were made in HEK cells, indicating that this propensity is general and not cell-type specific. In addition, the isolated NLS inhibited the import of full-length TAZ in a dose dependent manner, further confirming the importance of the identified NLS in the context of the intact protein (Figures 1D and S2A).

To verify that the requirement of the NLS for import is not restricted to the entry of the large 5C constructs, we quantified import of full-length TAZ 4SA and YAP 5SA labeled only with a single Citrine (Figure 1E). The uptake of these was faster relative to their export (as reflected by the higher steady state N/C) but

and with 4h LMB treatment (bottom). The scale bar represents 50 μm. Right: Quantification of the nuclear accumulation of the 5C-constructs upon LMB treatment for the indicated times. Median nucleocytoplasmic fluorescence ratios (median N/C of >100 cells) were determined for individual constructs as described previously[32] and data were fitted to mono-exponential growth curves with plateau. Number of repeats: 4.

(C) Localization of 5C-NLS constructs. Left: Representative fluorescence microscopy images of transfected LLC-PK1 cells. The scale bar represents 50 μm. Right: Quantification of the nuclear accumulation of 5C, 5C-TAZ NLS, 5C-YAP-NLS, and 5C-R5A in LLC-PK1 and HEK cells.

(D) The TAZ NLS inhibits the nuclear uptake of full-length TAZ. Cells were transfected with constant amounts of 5C or 5C-TAZ 4SA in combination with mCherry-TAZ NLS at ratios 1:0, 1:1, 1:2, 1:3, and 1:4. mCherry encoding vector was added to keep the total amounts of DNA constant. The increase in nuclear accumulation of 5C constructs after 6h LMB treatment, relative to no LMB addition is shown as ΔN/C (LMB). Number of repeats: 8. Also see Figure S2A.

(E) Localization of 1C constructs in LLC-PK1 and RPE-1 cells.

(F and G) Interaction between TAZ and IPO7. mCitrine (1C) and 1C-TAZ constructs were expressed in HEK cells. IPO7 (F) or Citrine-constructs (G) were immunoprecipitated and analyzed by western blotting using GFP- and IPO7 specific antibodies. Red asterisks indicate the position of relevant bands.

(H) Effect of ivermectin (iver; 25 μM) on the nuclear accumulation of endogenous TAZ/YAP and MRTF upon treatment with low calcium medium (LCM). Response is given as the percentage of uninhibited N/C increase at 60 min (TAZ/YAP) or 20 min (MRTF) LCM treatment.

(I) Nuclear accumulation of 5C-TAZ NLS and 5C-SV40 NLS in the presence of indicated concentrations of ivermectin. Also see Figure S2B.

(J) Effect of ivermectin on the nuclear accumulation of shuttling 5C-constructs induced by LMB treatment. ΔN/C (LMB) are calculated as in (D).

(K) Nuclear import of TAZ 4SA is Ran-independent. Cells were co-transfected with indicated constructs and non-related (siNR) or Ran-specific (siRan) siRNA and treated with LMB for 4h.

(L) Nuclear import of TAZ 4SA is ATP-independent. Left: Representative fluorescence microscopy images showing the effect of 2-deoxyglucose and azide on the cellular distribution of KPNA2. The scale bar represents 50 μm. Right: cells transfected with indicated constructs and treated for 4h with or without LMB, in the presence or absence of 2-deoxyglucose and azide. Means ± SD are depicted, and number of repeats are indicated. $^{*}p < 0.05$, $^{**}p < 0.01$, $^{***}p < 0.005$, $^{****}p < 0.001$; one-way ANOVA and Tukey-Kramer test.

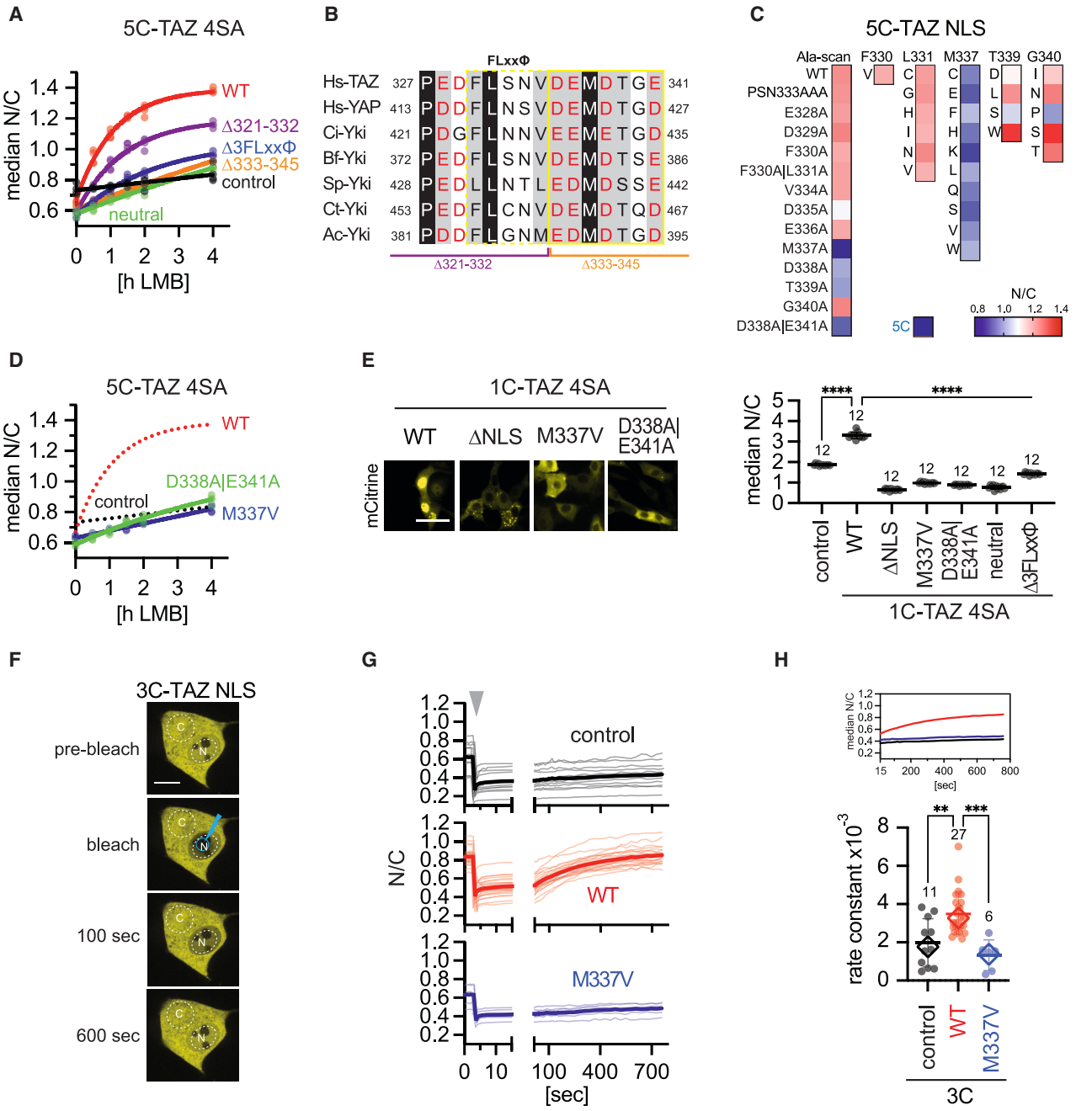

Figure 2. Characterization of the TAZ NLS

(A) LMB-induced nuclear accumulation of various 5C-TAZ 4SA constructs in LLC-PK1 cells, as described in Figure 1B. Δ3xFLxxΦ: 5C-TAZ 4SA with the three hydrophobic motifs FLxx[I,V,L,M] (including the PBM) mutated; neutral: 5C-TAZ 4SA with negatively charged residues at position 328, 329, 335, 336, 338, and 341 mutated to glycine; Δ321–332 and Δ333–345: 5C-TAZ 4SA constructs with deletions of the indicated regions, respectively. Number of repeats: 4.

(B) Sequence alignment of region 327–341 in human (Hs) TAZ with human YAP and orthologs (Yorkie, Yki) from sea slug (Ac: *Aplysia californica*), lancelet (Bf: *Branchiostoma floridae*), sea squirt (Ci: *Ciona intestinalis*), ringed worm (Ct: *Capitella teleta*), and sea urchin (Sp: *Strongylocentrotus purpuratus*). Positions with identical residues and conserved physicochemical properties are shown on black and dark gray background, respectively. Negatively charged residues are depicted in red. The hydrophobic motif FLxx[I,V,L,M] and the M-motif are boxed by dashed and solid yellow lines, respectively. Residues of the TAZ NLS missing in Δ321–332 and Δ333–345 constructs are indicated below.

(C) Point-mutational analysis of the TAZ NLS. Nuclear accumulation of 5C, 5C-TAZ NLS and mutants is depicted as heatmap. For N/C data points, see Figure S3.

(D) LMB-induced nuclear accumulation of 5C-TAZ 4SA constructs, as described in (A). Data points for WT and control are shown in (A) with fitting curves depicted as dotted lines for reference. Number of repeats: 4.

(legend continued on next page)

the deletion of the NLS still caused a drastic reduction in their nuclear accumulation. This was also true for the TAZ and YAP construct measured in RPE-1 cells.

We then assessed the contribution of IPO7-mediated transport under our conditions by deleting the PBM which is critical for IPO7 binding.[39] The ΔPBM constructs showed significantly less nuclear accumulation than their WT counterparts (Figures 1B and 1E), consistent with the reported role of this region in YAP import.[39] However, their nuclear import was still much higher than that of the respective ΔNLS constructs. These results prompted us to determine whether IPO7 could bind the isolated TAZ NLS and thereby contribute to its import. In immunoprecipitates of endogenous IPO7, we detected co-expressed 1C-TAZ 4SA while the 1C tag alone showed only background association (Figure 1F). Since bands from the precipitating antibody obscured potential signals from the 1C-TAZ NLS, we repeated the experiment using the 1C-tag for precipitation (Figure 1G). This setting showed that there was no association between the TAZ NLS and IPO7, whereas full-length TAZ bound IPO7. Thus, the TAZ NLS is necessary and sufficient to mediate import in an IPO7-independent manner.

Lastly, we wanted to address the role of the classic, importin α/β-dependent transport machinery in TAZ NLS import. To this end, we used ivermectin, an inhibitor of classic import. We first studied the ivermectin-sensitivity of endogenous TAZ/YAP in comparison to myocardin-related transcription factor (MRTF)[57,58] that is known to be taken up by classic nuclear import. We provoked their net nuclear uptake by low calcium-induced cell contact disruption, as reported.[7,11] Ivermectin at the usually applied concentration (25 μM) inhibited the nuclear accumulation of TAZ/YAP by ∼50%, consistent with the previously reported partial ivermectin sensitivity of wild-type TAZ.[38,40] Of note, ivermectin had a significantly stronger inhibitory effect on MRTF uptake (Figure 1H). We surmised that the residual TAZ/YAP import in the presence of ivermectin could be due to ivermectin-insensitive, non-classical mechanisms mediated by the TAZ NLS, in line with our earlier work.[32] Therefore, we measured the nuclear accumulation of 5C-TAZ NLS in the presence of increasing ivermectin concentrations. At 25 μM, the drug significantly reduced the nuclear accumulation of 5C-SV40 NLS, a construct bearing a monopartite NLS, while it did not influence the import of the TAZ NLS (Figure 1I). Even very high ivermectin concentrations (50 and 100 μM) had no discernable effect on TAZ NLS accumulation, in contrast to 5C-SV40 NLS. These results suggested that import mediated by the TAZ NLS is not ivermectin-sensitive (also see Figure S2B). Interestingly, 25 μM ivermectin did not affect the LMB-induced nuclear accumulation of 5C-TAZ 4SA, unlike that of the classic import probe 5C-R5A-NES (Figure 1J) indicating that, under our conditions, the monitored nuclear uptake of 5C-TAZ 4SA depends predominantly on the TAZ NLS driven import. This is in agreement with our deletion experiments (Figure 1B). In line with this interpretation, Ran knockdown significantly inhibited classic import but did not affect the LMB-induced nuclear uptake of TAZ 4SA (Figure 1K). Finally, we treated cells with sodium azide and 2-deoxyglucose, which has been shown to deplete free ATP, GTP and GTP-loaded Ran levels in cells, thereby inhibiting classic protein import and redistributing importin α into the nucleus.[59] Upon ATP depletion, we indeed observed dramatic nuclear accumulation of importin α, with a concomitant inhibition of classic protein import, as measured by the reduced nuclear accumulation of 5C-R5A-NES (Figure 1L). However, ATP depletion did not affect the import of TAZ 4SA. Taken together, the unconventional NLS represents a distinct and indispensable import motif underlying the facilitated but Ran/ATP-independent nuclear uptake of TAZ/YAP. As such, it warranted further in-depth analysis.

Critical determinants of the TAZ NLS function

In our earlier work, we identified three hydrophobic FLxx(V/L/I/M) motifs important for TAZ nuclear accumulation that are located in the NLS, between residues 340–346 and in the C-terminal PBM.[32] While mutation of all three motifs (5C-TAZ 4SA Δ3FLxxΦ) abolished nuclear import (Figure 2A), deletion of the motif within the NLS (5C-TAZ 4SA Δ321-332) had only a moderate effect. This finding suggested that the N-terminal half of the NLS, including the hydrophobic motif, did not harbor the most critical determinants for import. Therefore, we set out to characterize the TAZ NLS in greater detail. The C-terminal half of the NLS comprises four conserved negatively charged residues, flanking a highly conserved methionine (Figure 2B). Deletion of this half (5C-TAZ 4SA Δ333-345) inhibited import to the same extent as the deletion of the full NLS (Figures 2A and 1B). Likewise, substitution of the negatively charged residues in the NLS with glycine (5C-TAZ 4SA neutral), eliminated nuclear accumulation.

In a systematic analysis, we mutated each residue in the 5C-tagged TAZ NLS to alanine, either alone or in combination, which further confirmed that the second half of the NLS comprised the key residues necessary for import (Figure 2C, see also Figure S3). Alanine mutation of D335, D338, or T339 significantly reduced import, whereas constructs with double mutation D338A|E341A eliminated it. Remarkably, mutation M337A alone was sufficient to localize the mutant NLS to the cytoplasm.

Next, we determined which are the essential physicochemical properties at individual, non-charged positions. Mutating residues belonging to the hydrophobic motif (F330, L331) was

(E) Nuclear accumulation of 1C-TAZ 4SA constructs. WT refers here to the parental 1C-TAZ 4SA plasmid. Representative microscopy images depicted on the left. The scale bar represents 50 μm. Control: Citrine.

(F–H) FRAP-Analysis of TAZ nuclear import. (F) Illustration of FRAP based nuclear import studies. The initial nuclear (N) to cytoplasmic (C) mean fluorescence ratio of 3C-TAZ NLS and its recovery after bleaching the nuclear compartment was measured. The scale bar represents 10 μm. For the steady-state distribution of 3C constructs, see Figure S4. (G) 3C-constructs were expressed in LLC-PK1 cells and nuclear fluorescence was reduced by ca 30–50% using a bleaching laser to minimize photodynamic damage (arrowhead). Fluorescence in the nuclear and cytoplasmic compartment was monitored for ca 800 s and the N/C were plotted against time. Recovery curves of individual cells and an average curve are shown as thin and bold lines, respectively. Recovery curves were fitted to a mono-exponential function, excluding early time points (<15 s) where intranuclear diffusion convolutes fluorescence recovery by import. Number of repeats: 11, 27 and 6 for control, 3C-TAZ NLS and 3C-TAZ NLS M337V, respectively. (H) Top: overlay of average recovery curves. Bottom: Rate constants of mono-exponential fitting curves for individual cell recoveries and the averaged recovery are plotted as spheres and diamonds, respectively. Means ± SD are depicted, and number of repeats are indicated. *$p < 0.05$, **$p < 0.01$, ***$p < 0.005$, ****$p < 0.001$; one-way ANOVA and Tukey-Kramer test.

inconsequential (Figure 2C), consistent with the behavior of the Δ321-332 TAZ construct (Figure 2A). Residue T339 could be replaced with large, hydrophobic residues (Leu, Trp) without loss of function. Residue G340 tolerated substitution with various amino acids, only proline reduced nuclear accumulation. In contrast, all tested replacements for M337, even the semi-conservative mutations M337L and M337V, disrupted import. We then introduced the point mutations D338A|E341A or M337V into full-length TAZ to evaluate their impact on nuclear accumulation of the otherwise intact protein. The mutants failed to accumulate in the nucleus both as 5C- and 1C- construct (Figures 2D and 2E).

Finally, we sought to reaffirm the critical importance of the single methionine by using dynamic transport measurement in live cells, based on 3C-TAZ NLS constructs with a size comparable to 1C-TAZ. For this, we monitored the import of control (3C), TAZ NLS, and the M337V mutant using fluorescence recovery after photobleaching (FRAP) (Figure 2F, also see Figure S4). After photobleaching of nuclear fluorescence, 3C and 3C-TAZ NLS M337V essentially failed to recover, while 3C-TAZ NLS exhibited near-complete recovery (Figures 2G and 2H).

Taken together, we found that the C-terminal part of region 327–341 harbors the major determinants of the unconventional TAZ NLS: negative charges flanking a conserved methionine, to which we refer to as "M-motif".

M-motif in cellular proteins: A novel import-competent signature

An important question is whether the M-motif NLS is specific to TAZ/YAP, or whether it also mediates nuclear import of other proteins. To identify such proteins, we searched the literature for Ran-, importin α/β-, and energy-independent nuclear import, similar to that of the TAZ NLS. Candidate proteins were then assessed for the presence of a methionine with flanking negative charges – present directly or attained via phosphorylation (details in STAR Methods). We found that STAT1, cyclin B1, and hnRNP K met these criteria[60–64] (Figures 3A and S5A). Similar to TAZ and YAP, regulation of STAT1, cyclin B1, and hnRNP K nuclear presence is tightly linked to their biological activities.[64–71]

STAT1 is a transcription factor that regulates inflammatory/immunological (e.g., antiviral) responses.[65,72,73] Antiviral signaling triggers tyrosine phosphorylation and importin α-mediated nuclear import of STAT1.[74] However, continuous nucleocytoplasmic shuttling of unphosphorylated STAT1 has been implicated both in interferon-related and unrelated functions.[60,75] Remarkably, we identified an M-motif (residues 689–695) in the linker between SH2 domain and the SH2-binding site, raising the possibility that it could mediate transport of the unphosphorylated STAT1. Figures 3A and 3B show that a 5C-STAT1 fragment containing this M-motif NLS accumulated in the nucleus, in contrast to the M/V mutant version (M691V). Interestingly, mutation of M691V is associated with Mendelian susceptibility to mycobacterial disease, and it compromises nuclear localization of STAT1.[76] Like TAZ (Figure 1D), the nuclear localization of GFP-STAT1 was reduced upon coexpression of the TAZ NLS, but not the M337V variant (Figure 3C). These results suggest that STAT1 undergoes M-motif dependent nuclear import.

Cyclin B1 is a master regulator of the cell cycle that initiates the onset of mitosis upon accumulation in the nucleus.[66–68] Its M-motif includes phosphorylation sites S126, S128 and S133 (Figures 3A and 3D top) which stimulate cyclin B1 import when phosphorylated.[77] Accordingly, the unmodified 5C-tagged cyclin B1 fragment exhibited only weak nuclear import capacity. However, when we mutated the serine residues to glutamate, a potent phospho-Ser-mimic,[77] the resultant fragment 5C-3SE accumulated strongly in the nucleus (Figure 3A). Importantly, this transport was methionine-dependent; 5C-3SE M/V remained cytoplasmic. Therefore, cyclin B1 comprises a phosphorylation-regulated M-motif. To confirm the import function of the M-motif when embedded in its natural sequence context, we studied the transport behavior of the so-called cytoplasmic retention signal (CRS) of cyclin B1[77,78]. This region comprised the M-motif NLS, a NES and altogether five phosphorylation sites (Figure 3D). LMB treatment to inhibit NES-driven efflux induced relatively weak import of 5C-CRS, strong import of the respective phosphomimetic mutant 4SE and only residual import of the 4SE M/V mutant (Figures 3E, 3F, and S5B), confirming that the post-translationally regulated M-motif is also functional within the CRS. Moreover, our results broaden our understanding of how phosphorylation induces nuclear accumulation of cyclin B1: phosphorylation of residues S126, S128 and S133 establishes a functional M-motif NLS, whereas phosphorylation of site S147 diminishes the function of the surrounding NES.[79]

hnRNP K is involved in the nuclear export of mRNA and can act as a transcription factor and as such, shuttles between nucleus and cytoplasm utilizing a short fragment named KNS (Figure 3D bottom).[64,69–71] We tested the potential M-motif NLS in the KNS (Figure 3A) for methionine- and charge-dependent import. For this, we utilized our RIS'N (Rapamycin Induced Sequestration in the Nucleus) system[32] (Figure 3G). In short, rapamycin induces the sequestration of a 5C-FRB tagged protein within the nucleus through linking the FRB domain to an FKBP-anchor construct (H2B-2xFKBP-mCherry). Due to the large tag, the protein can only accumulate in the nucleus when it contains a licensing NLS. Accordingly, rapamycin induced substantial accumulation of 5C-FRB-KNS over the 5C-FRB tag alone (Figure 3H, also see Figure S5C), and mutation of the C-terminal methionine (M359V), or of negatively charged central residues to glycine (neutral), significantly reduced nuclear accumulation. Therefore, the KNS mediated import through the action of an M-motif variant. In conclusion, we identified functional M-motif NLS in three other proteins, in addition to TAZ and YAP. Therefore, we propose that the M-motif signifies a general, new class of NLS.

Viral M-motifs share functional similarities with the TAZ M-motif: Import capacity and RAE1 binding

We noticed that the viral proteins VSV-M, rift valley fever virus non-structural protein S (RVFV-NSs), SARS2-ORF6, and SARS-ORF6, amongst others, contain sequence signatures conforming to the TAZ/YAP M-motif (Figures 4A and S5D). Therefore, we asked if viral M-motifs can mediate nuclear import (NLS function) and/or it can affect the uptake of host M-motif proteins (e.g., TAZ/YAP). To address this, we generated fusion proteins comprising 5C and the corresponding isolated viral M-motifs or full-length viral proteins. All tested viral signatures

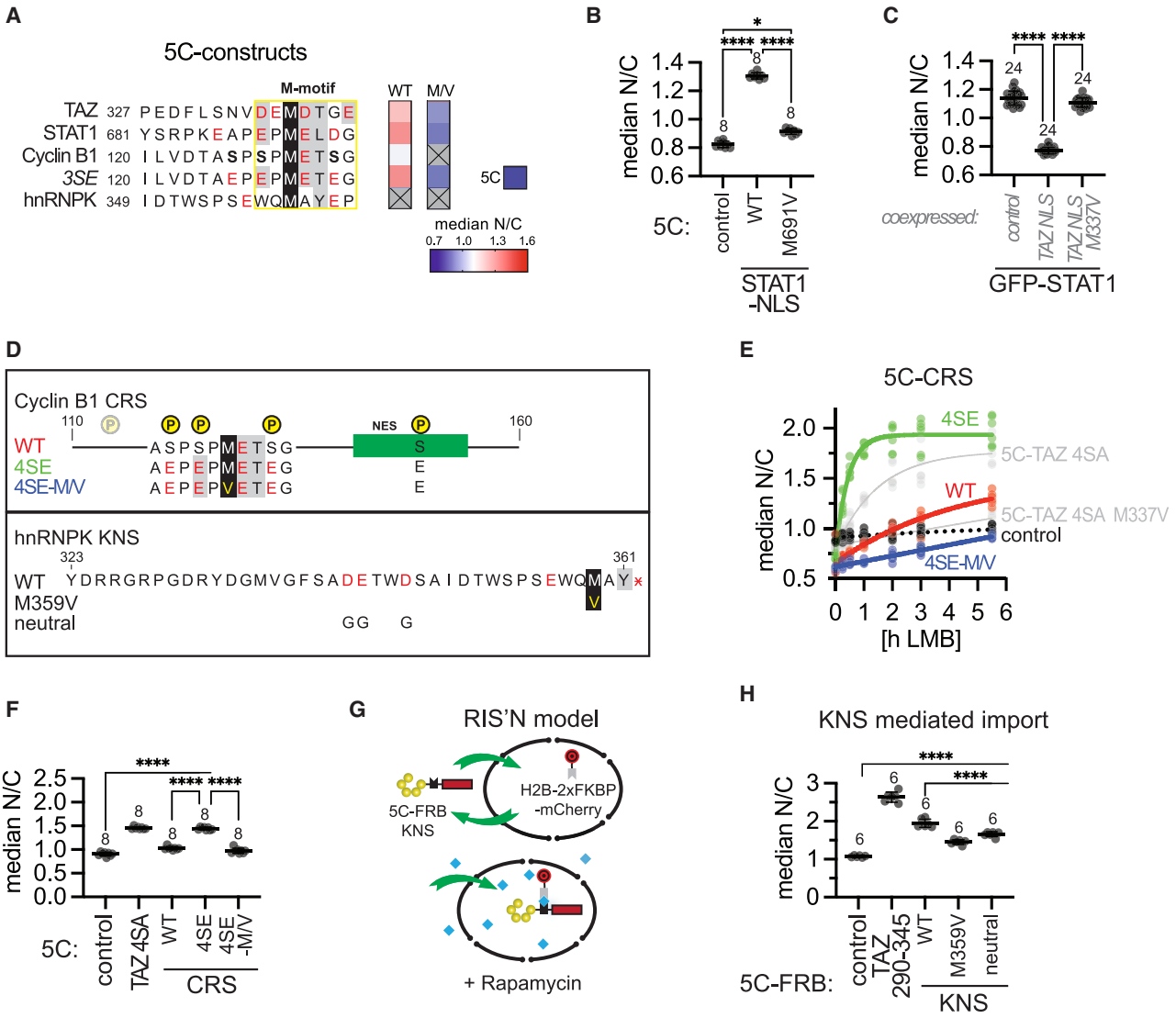

Figure 3. M-motif signatures in cellular proteins with known, non-canonical nuclear import

(A) Sequence alignment (left) of the human TAZ NLS (region 327–341) with human STAT1 "Uniprot: P42224", cyclin B1 "Uiprot: P14635", the phosphomimic cyclin B1 mutant 3SE and hnRNPK "Uniprot: P61978". Residues conforming to the M-motif signature [DE]xM[DE][TLIVMWFY]x[DE] (Figure 2C) are depicted on gray and black background and the string is boxed in yellow. Negatively charged residues within the signature or in proximity are depicted in red. Right: Heatmap of the nuclear accumulation of 5C, 5C-TAZ NLS and 5C-tagged fragments of STAT1, Cyclin B1 and hnRNPK and of the corresponding methionine-to-valine mutants. Peptides not tested are indicated by gray, crossed boxes. For N/C data points, see (B) and Figure S5A.

(B) Individual data points of 5C, 5C-tagged wild-type and M691V STAT1 fragment (STAT1-NLS) nuclear accumulation, shown as heatmap in (A).

(C) The TAZ NLS but not the M337V mutant reduces the steady-state nuclear presence of STAT1. GFP-STAT1 was coexpressed with mCherry (control), mCherry-TAZ NLS or mCherry-TAZ NLS M337V. Coexpressed constructs are indicated in gray italics.

(D) Features and mutations of CRS and KNS, with M-motif residues and proximal negatively charged residues depicted as in (A). Important phosphorylation sites are highlighted by a yellow encircled P and the NES is depicted as green box.

(E) Nuclear accumulation of 5C-CRS and TAZ constructs when treated with LMB for increasing times. The black dotted line marks the N/C fitting curve of 5C (control). The number of repeats is 5 for 5C-CRS WT, timepoints 0, 0.25, and 0.5h; for all others it is 6.

(F) Nuclear accumulation of 5C-CRS and TAZ constructs after 5h LMB treatment. Also see Figure S5B.

(G) RIS'N model showing rapamycin-induced nuclear entrapment of 5C-FRB-KNS by H2B-2xFKBP-mCherry, as described previously.[32]

(H) Nuclear accumulation of 5C-FRB, 5C-FRB-TAZ 290–245 and 5C-FRB-KNS constructs after 6h rapamycin treatment. Also see Figure S5C. Means ± SD are depicted, and number of repeats are indicated. *$p < 0.05$, **$p < 0.01$, ***$p < 0.005$, ****$p < 0.001$; one-way ANOVA and Tukey-Kramer test.

accumulated in the nucleus in a methionine-dependent manner (Figure 4A), as did the tested 5C-tagged full-length proteins RVFV-NSs and SARS2-ORF6 (Figure 4B). Further, the isolated M-motif as well as full-length SARS2-ORF6 could diminish nuclear accumulation of 5C-TAZ NLS, 5C-TAZ 4SA and endogenous TAZ and YAP (Figures 4C–4E).

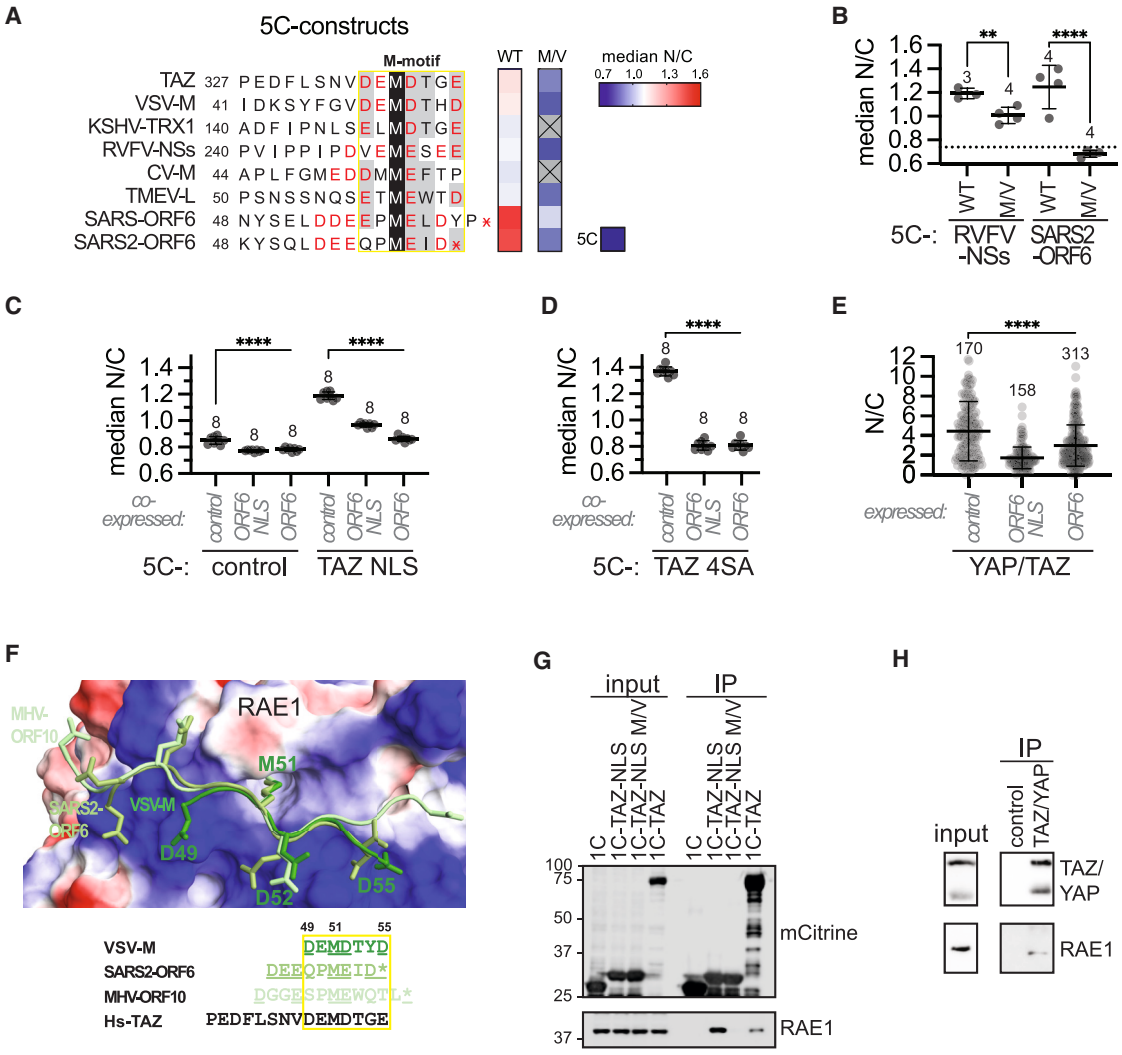

Figure 4. Viral M-motifs share functional similarities with the TAZ M-motif: import capacity and RAE1 binding

(A) Alignment of the human TAZ NLS with viral proteins and nuclear accumulation of 5C, 5C-TAZ NLS and 5C-tagged viral fragments depicted as heatmap, as described in Figure 3A. For data points, see Figure S5D. CV-M: Chandipura virus matrix protein "Uniprot: Q9WH76"; KSHV-TRX1: Kaposi's sarcoma-associated herpesvirus triplex capsid protein 1 "Uniprot: F5H8Y5"; RVFV-NSs: rift valley fever virus non-structured protein NSs "Uniprot: P21698"; SARS2-ORF6: severe acute respiratory syndrome coronavirus 2 ORF6 protein "Uniprot: P0DTC6"; SARS-ORF6: severe acute respiratory syndrome coronavirus ORF6 protein "Uniprot: P59634"; TMEV-L: Theiler's murine encephalomyelitis virus leader protein "Uniprot: P13899"; VSV-M: vesicular stomatitis virus matrix protein "Uniprot: Q8B0H7".

(B) Nuclear accumulation of 5C-tagged full-length viral proteins. The black dotted line marks the mean N/C of 5C.

(C) Inhibition of TAZ NLS nuclear import by full-length SARS2-ORF6 or its NLS. mCherry (control), mCherry-tagged SARS2-ORF6 or SARS2-ORF6-NLS were cotransfected with indicated 5C-constructs and nuclear localization was quantified.

(D) Inhibition of LMB-induced 5C-TAZ 4SA nuclear import by SARS2-ORF6 and its M-motif.

(E) Inhibition of endogenous TAZ/YAP import by SARS2-ORF6 and its M-motif.

(F) Structural superposition of RAE1–MHV-ORF10 (PDB: 7BYF), RAE1– SARS2-ORF6 (PDB: 7VPH) and RAE1–VSV-M (PDB: 4OWR). The surface representation of murine RAE1 (PDB: 7BYF) is colored according to the vacuum electrostatic potential ranging from red to blue for negative to positive values. Fragments of MHV-ORF10, SARS2-ORF6 and VSV-M proteins are depicted as cartoons in pale, smudge and forest green, respectively, with selected sidechains shown as stick models. An alignment of the fragments and the TAZ NLS are shown below.

(G) Interaction between TAZ and RAE1. 1C and 1C-TAZ constructs were expressed in HEK cells, immunoprecipitated with GFP-trap beads, and analyzed by western blotting using GFP- and RAE1-specific antibodies.

(H) Interaction between endogenous TAZ and RAE1. Immunoprecipitations with unspecific IgG antibody (control) or a TAZ/YAP-specific antibody from LLC-PK1 lysates and subsequent western blotting using TAZ/YAP- and RAE1-specific antibodies. Means ± SD are depicted, and number of repeats are indicated. $^{**}p < 0.01$, $^{****}p < 0.001$; one-way ANOVA and Tukey-Kramer test.

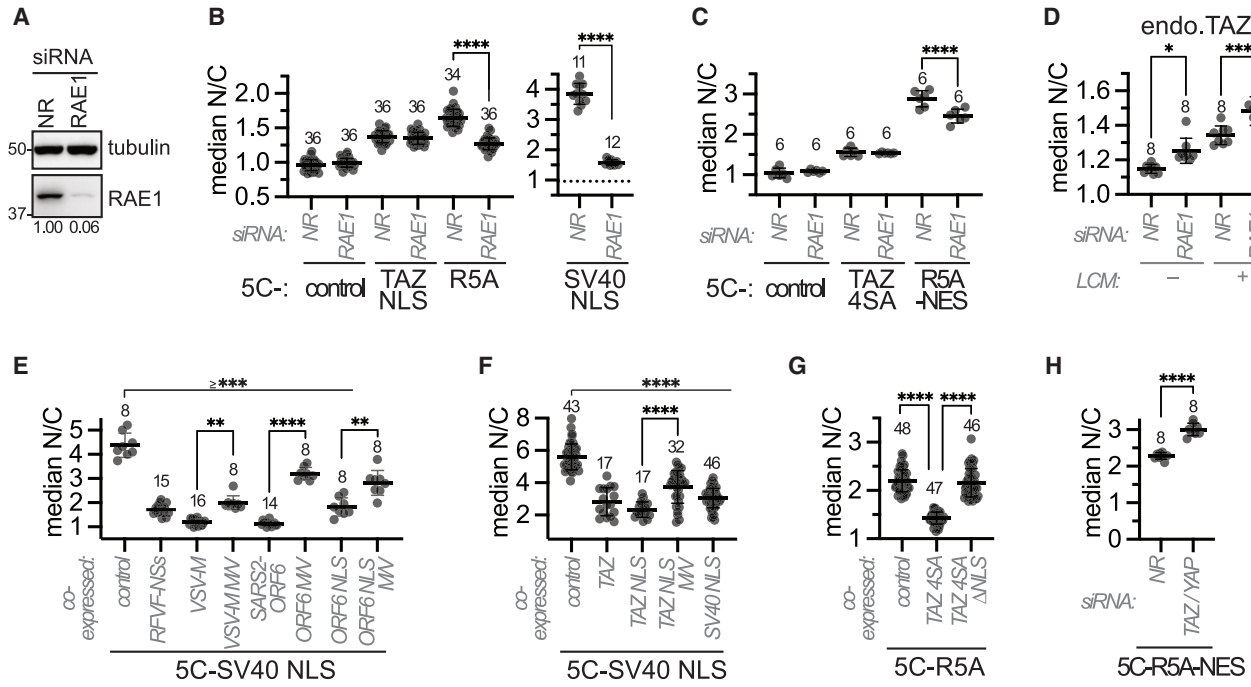

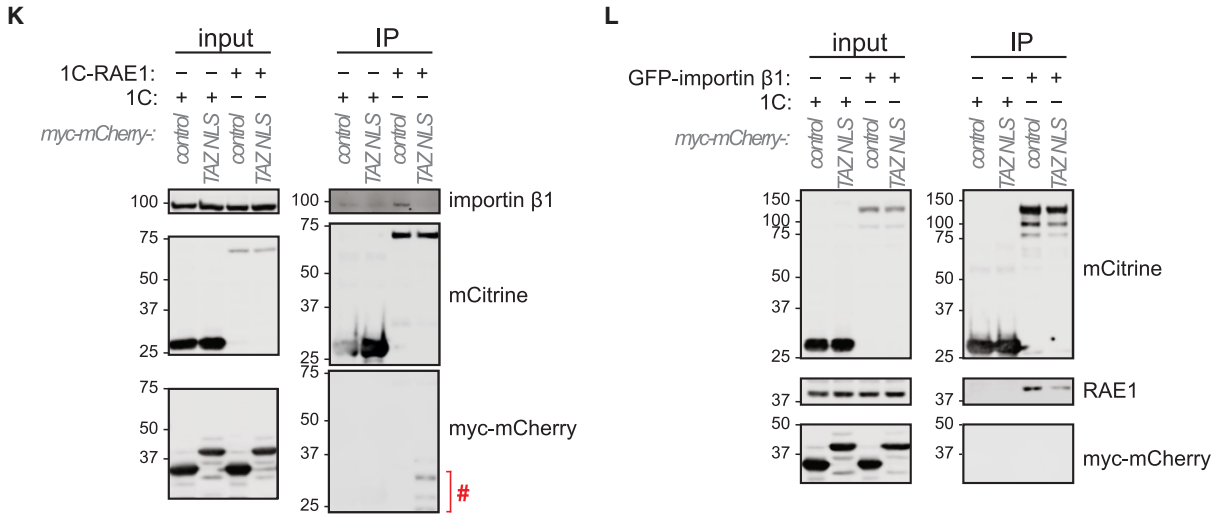

(legend on next page)

The target of viral M-motifs is RAE1, a protein which localizes to the nuclear pore complex and associates with the pore component Nup98.[80–85] Binding between viral M-motifs and the RAE1/Nup98 complex involves both the central methionine and the surrounding negative charges. Specifically, the methionine sidechain tightly snugs into a hydrophobic pocket of RAE1 while the flanking acidic residues form electrostatic interactions with basic residues surrounding the hydrophobic pocket (see crystal structure in Figure 4F). This prompted us to test whether the TAZ M-motif can also associate with RAE1. As shown in Figure 4G, immunoprecipitation of the tagged TAZ NLS and full-length TAZ coprecipitated endogenous RAE1 while the TAZ NLS M/V mutant did not. Correspondingly, endogenous TAZ and RAE1 also interacted (Figure 4H). Thus, the TAZ M-motif, similar to its viral counterparts, can bind RAE1.

Taken together, the tested viral sequences constitute transport-competent M-motif NLS and have the capacity to interfere with M-motif NLS in host proteins (see discussion). These observations are all compatible with and likely due to a competitive type of inhibition, although other mechanisms of action cannot be excluded. Further, while the viral M-motifs are undoubtedly capable of catalyzing nuclear import, their functional significance with regards to the corresponding viral proteins remains to be elucidated. Indeed, many of them accumulate in the nuclear envelope (just like RAE1) rather than within the nucleus, pointing to a stabilized association between the viral proteins and the nuclear membrane. The RAE1–M-motif interaction is certainly necessary for this,[80–82,86] but it is likely not sufficient; rim accumulation requires additional viral sequences. Correspondingly, while the tested full-length viral proteins (VSV-M and RVFV-NSs), show predominant and methionine-dependent rim staining, the isolated M-motifs (of either ORF6 or TAZ) and full-length TAZ failed to do so (Figure S6).

RAE1 is not necessary for nuclear TAZ import but contributes to classic protein import

RAE1, a mobile nuclear pore component, is a key target of many viruses through which they interfere with host nuclear transport processes to boost their propagation.[15,44–52,87] These facts together with our finding that TAZ can bind RAE1 raised two, mutually non-exclusive possibilities. First, that RAE1 might mediate the nuclear import of TAZ. Second, that TAZ might inhibit classic nuclear transport, and RAE1 might play a role in this process. The following experiments address these possibilities. To assess the role of RAE1 in TAZ import, we transfected cells with a RAE1-specific siRNA. This treatment dramatically reduced RAE1 levels (Figure 5A) but it failed to inhibit the steady state nuclear accumulation of the TAZ NLS (Figure 5B). It also did not alter the Leptomycin B-induced net nuclear accumulation of full-length TAZ 4SA (Figure 5C and see Figure S7A). Moreover, RAE1 downregulation did not reduce but rather increased the low calcium-induced import of endogenous TAZ (Figure 5D). These findings strongly suggest that RAE1 is not required for TAZ import, contrary to our expectations. In contrast, RAE1 knockdown clearly mitigated uptake of classic NLS (Figures 5B and 5C), implicating RAE1 in importin α/β-dependent protein import. This finding prompted us to characterize the impact of M-motifs and TAZ itself on classic protein import.

TAZ inhibits classic protein import via its M-motif, similar to viral M-motifs

As mentioned, viral M-motif proteins were shown to suppress antiviral responses, partly via their capacity to interfere with nuclear transport, including protein import.[44–52,87–94] First, we wished to test if various viral M-motif proteins or M-motifs can indeed inhibit classic nuclear import of proteins in our system. Coexpression of VSV-M, RVFV-NSs, SARS2-ORF6, as well as SARS2-ORF6 M-motif reduced import of 5C-SV40 NLS (containing a classic NLS), and this occurred in a methionine-dependent manner (Figure 5E). Importantly, we also found that both the TAZ NLS and full-length TAZ potently reduced classic protein import (Figures 5F and 5G). This effect was lost by deleting the NLS from full-length TAZ, and it was significantly reduced by mutating the methionine in the TAZ NLS. Of note, mutational analysis showed that the key residues necessary for TAZ import itself (methionine, negative charges) were overlapping with those required for the inhibition of classic import and RAE1 binding (see Figure S7B). Importantly, silencing endogenous TAZ/YAP augmented classic protein import (Figures 5H and S7C). Taken together, these findings imply that TAZ, via its M-motif NLS has a potent capacity to inhibit classic protein import.

Figure 5. Classic protein import into the nucleus: role of RAE1 and inhibition by viral proteins and TAZ

(A) Confirmation of RAE1 knockdown, tested by western blot with a RAE1-specific antibody and tubulin as loading control. RAE1 band intensities were normalized to the non-related siRNA control (NR) and are shown below the blot.

(B and C) Nuclear accumulation of indicated 5C constructs, when cotransfected with NR or RAE1-specific siRNA. The black dotted line marks the mean N/C of 5C, cotransfected with siNR. Also see Figure S7A.

(D) Nuclear accumulation of endogenous (endo.) TAZ in cells, transfected with indicated siRNA and with or without LCM stimulation. N/C was determined using a TAZ-specific antibody on fixed cells.

(E and F) Nuclear accumulation of 5C-SV40-NLS when coexpressed with mCherry (control) or the indicated mCherry fusion proteins.

(G) Nuclear accumulation of 5C-R5A, when coexpressed with myc-mCherry (control) or the indicated myc-TAZ constructs.

(H) LMB-induced nuclear accumulation of 5C-R5A-NES, when cotransfected with NR or TAZ/YAP-specific siRNA. Also see Figure S7C.

(I and J) The TAZ NLS reduces cargo-importin interactions. (I) 5C-SV40 NLS was coexpressed with mCherry (control) or mCherry-TAZ NLS in HEK cells, immunoprecipitated with GFP-trap beads, and analyzed by western blotting using GFP-, importin α1- or importin β1-specific antibodies. (J) Quantification of the binding of importins to cargo (5C-SV40 NLS) upon coexpression of indicated constructs. Cargo binding in the presence of TAZ NLS was normalized to the binding in the presence of control construct and the statistical significance was calculated using a one-sample t test.

(K and L) The TAZ NLS reduces RAE1-importin β1 interaction. 1C, 1C-RAE1 or GFP- importin β1 was coexpressed with myc-mCherry (control) or myc-mCherry-TAZ NLS in HEK cells, immunoprecipitated with GFP-trap beads, and analyzed by western blotting using GFP-, myc-, importin β1- or RAE1-specific antibodies. Red hashtag marks myc-mCherry-TAZ degradation products. Means ± SD are depicted, and number of repeats are indicated. *$p < 0.05$, **$p < 0.01$, ***$p < 0.005$, ****$p < 0.001$; one-way ANOVA and Tukey-Kramer test.

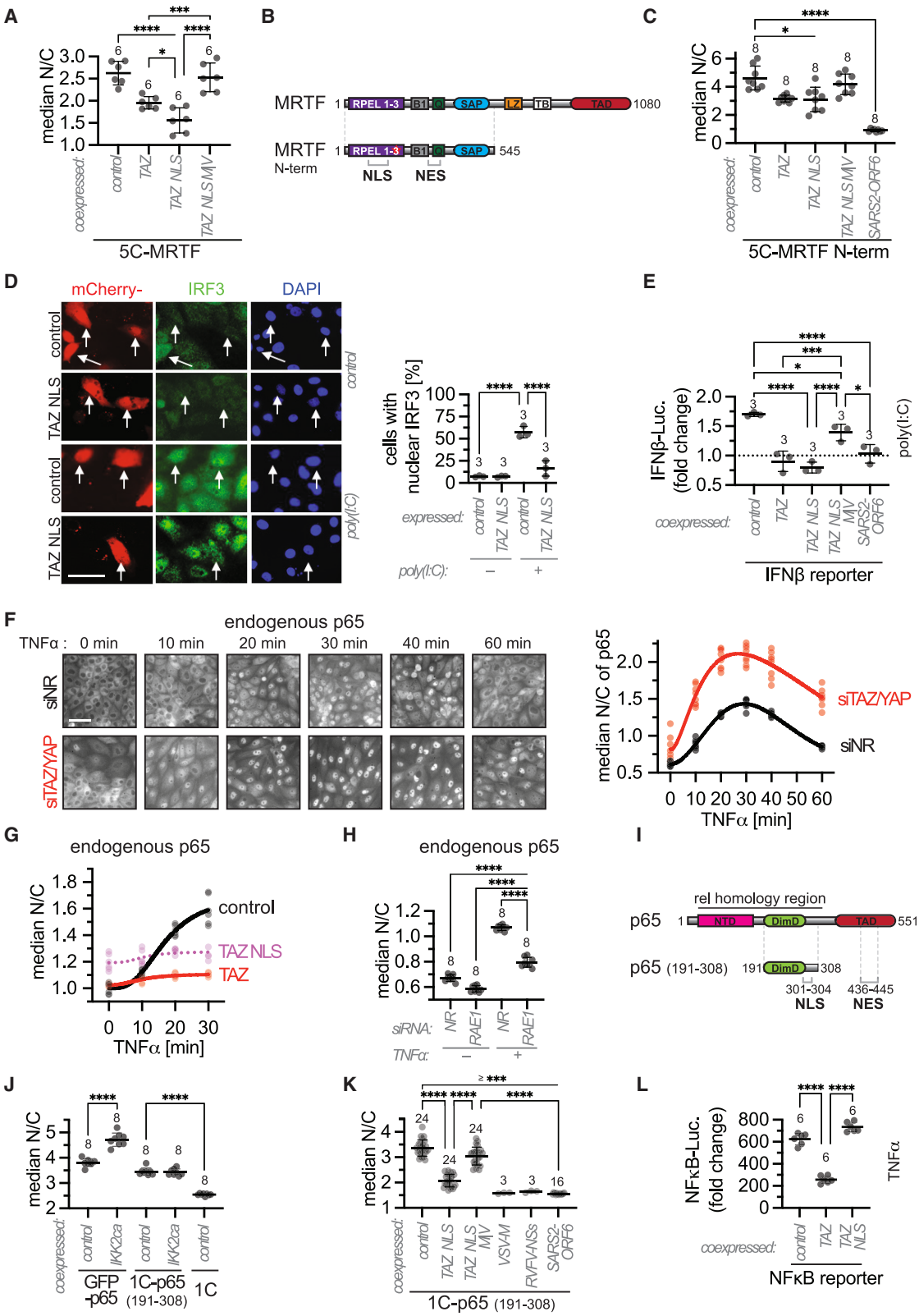

(legend on next page)

Next, we sought to gain insight into the underlying mechanism. Co-immmunoprecipitation experiments revealed that expression of the TAZ NLS reduced the association of 5C-SV40 NLS with importin α and β1 (Figures 5I and 5J). We then tested if RAE1 can be integrated into this inhibitory mechanism. This was plausible since RAE1 was reported to bind importin β1.[95] Indeed, RAE1 pulldown co-precipitated importin β1, and the TAZ-NLS reduced this association (Figure 5K). Conversely, importin β1 pulldown resulted in the co-precipitation of RAE1, which was mitigated by TAZ-NLS expression (Figure 5L). Thus, disassembly of complexes containing RAE1 and importin β1 is a possible mechanism whereby TAZ can interfere with classic protein transport. This interpretation is reinforced by a recent report, showing the dissociation of importin α and β from the Nup98/RAE1 complex by ORF6.[96] Nonetheless, further studies are needed to clarify the exact molecular mechanism. Taken together, TAZ via its M-motif emerges as a potent inhibitor of classic nuclear import, at least in part in a RAE1-dependent manner.

TAZ and the TAZ NLS inhibit the nuclear import of cellular proteins, including key antiviral transcription factors

Having shown that TAZ can inhibit classic protein import, we wished to address the potential (patho)physiological significance of this finding by looking at natural cellular cargoes. We first focused on the nuclear transport of MRTF because it shows crosstalk with TAZ in fibrogenesis, and we have demonstrated earlier that TAZ can inhibit its nuclear localization.[7] However, the potential contribution of nuclear import inhibition (in addition to direct binding and cytosolic retention) has not been investigated. TAZ and the TAZ NLS, but not the TAZ NLS M/V mutant decreased nuclear localization of 5C-MRTF (Figure 6A, also see Figure S8A). Since the C-terminal half of MRTF can directly interact with TAZ, promoting cytoplasmic sequestration,[7] we repeated the experiment with the corresponding C-terminal deletion construct 5C-MRTF-N-term (Figure 6B). This construct was constitutively nuclear due to mutation R137A in the RPEL motif which abolishes actin binding and the consequent masking of a classic NLS. Strikingly, TAZ and the TAZ NLS, as well as SARS2-ORF6, were still able to reduce nuclear accumulation of 5C-MRTF-N-term (Figure 6C). These results demonstrated that TAZ negatively impacts the nuclear import of MRTF as an additional factor in the multilevel interplay between these transcriptional co-activators.[7]

The second set of proteins we studied were the transcription factors IRF3 and NF-κB p65 because they play key roles in antiviral responses, which were shown to be blunted by TAZ and YAP.[53–55] Strikingly, this capacity of TAZ and YAP resembles the action of the viral suppressors VSV-M and SARS2 ORF6.[47–52,87,88,92] Based on our results, we suspected that TAZ could directly interfere with IRF3 and NF-κB p65 importin α/β-dependent nuclear import, in addition to the block of upstream signaling. To activate the IRF3 signaling pathway, we stimulated cells with polyinosinic:polycytidylic acid, poly(I:C), a structural mimetic of double-stranded (viral) RNA. This stimulus triggered the nuclear uptake of endogenous IRF3, which could be abolished by overexpression of the TAZ NLS (Figure 6D). Similarly, poly(I:C) stimulated IRF3 transcriptional activity, as measured by a IFNβ luciferase reporter construct, and this effect was reduced by overexpressed TAZ NLS, as well as full-length TAZ and SARS2-ORF6 (Figures 6E and S8B). These results are consistent with the proposed inhibitory effect of the TAZ NLS on IRF3 nuclear import and suggest that TAZ reduces antiviral responses, partly by directly inhibiting the nuclear import of IRF3.

For studying classic nuclear import of endogenous NF-κB[97,98], cell were treated with TNFα. In cells transfected with control siRNA, TNFα triggered transient nuclear uptake of NF-κB p65 (Figure 6F). This uptake was enhanced and prolonged when TAZ and YAP were downregulated, in agreement

Figure 6. TAZ inhibits the import of transcription factors known to functionally interact with TAZ

(A) Nuclear accumulation of 5C-MRTF, when cotransfected with mCherry (control) or the indicated mCherry-fusion proteins. Also see Figure S8A.

(B) Domain organization of MRTF and MRTF N-term. B1: basic region 1; Q: Q-rich region; SAP: SAF-AIB, Acinus, Pias domain; LZ: leucine zipper motif; RPEL: RPEL domain; TAD: transcription activation domain; TB: TAZ binding site (PPxY motif). A red star indicates mutation R137A. NLS and NES are shown below.

(C) Nuclear accumulation of 5C-MRTF N-term, when cotransfected with indicated mCherry constructs.

(D) Nuclear accumulation of endogenous IRF3 in cells transfected with mCherry (control) or mCherry-TAZ NLS with or without stimulation by poly(I:C). Left: representative fluorescence microscopy images with mCherry positive cells indicated by white arrows. The scale bar represents 50 μm. Right: percentage of transfected cells with nuclear IRF3, quantified from three independent experiments.

(E) Measurement of IRF3 transcriptional activity in cells transfected with indicated constructs and treated with poly(I:C), using an IFNβ promoter luciferase reporter construct. Values are normalized to the unstimulated control, indicated by the black dotted line. Also see Figure S8B.

(F) Nuclear accumulation of endogenous NF-κB p65 in cells transfected with NR or TAZ/YAP-specific siRNA, upon TNFα treatment for indicated times. Left: representative fluorescence confocal microscopy images. The scale bar represents 50 μm. Right: quantification of nuclear accumulation. Number of repeats: 8.

(G) Nuclear accumulation of endogenous NF-κB p65 in cells transfected with the indicated mCherry fusion proteins, upon TNFα treatment for indicated times. The number of repeats is 4 for mCherry-TAZ NLS (30 min); 5 for control (10 min) and mCherry-TAZ (30 min); for all others 6.

(H) Cells were transfected with NR or RAE1-specific siRNA and either stimulated for 30 min with TNFα or left unstimulated. Nuclear accumulation of endogenous p65 was determined using a specific antibody on fixed cells.

(I) Domain organization of NF-κB p65 and the signaling-independent fragment 191–308. NTD: N-terminal domain; DimD: dimerization domain; TAD: transactivation domain. The region encompassing the rel homology domain is shown above, NLS and NES below, also see Figure S8C.

(J and K) Nuclear accumulation of GFP-p65, 1C-p65 (191–308) or 1C, when cotransfected with mCherry (control), constitutive active IKK2 (IKK2ca), or the other indicated mCherry fusion proteins; also see, Figure S8D.

(L) Measurement of NF-κB p65 transcriptional activity in cells transfected with indicated constructs and treated with TNFα, using an NF-κB promoter luciferase reporter construct. Values are normalized to the unstimulated control; see also Figure S8E. Means ± SD are depicted and number of repeats are indicated. *$p < 0.05$, ***$p < 0.005$, ****$p < 0.001$; one-way ANOVA and Tukey-Kramer test.

with published results.[53] Conversely, expression of full-length TAZ effectively inhibited TNFα-induced NF-κB p65 nuclear uptake (Figure 6G). Interestingly, the TAZ NLS slightly increased basal nuclear presence of NF-κB p65, yet, it suppressed TNFα-mediated further induction. Moreover, in agreement with our earlier findings, RAE1 downregulation also decreased TNFα-induced nuclear accumulation of endogenous NF-κB p65 (Figure 6H).

Since diminished nuclear accumulation might also be due to reduced upstream signaling, we generated a "signaling-independent" p65 construct (1C-tagged fragment 191–308). It comprises the dimerization domain and the functional, classic NLS of NF-κB p65 (Figure 6I) driving nuclear accumulation (Figures S8C and S8D), but lacks the N- and C-terminal regions which are required for the expression and high affinity binding of its inhibitor IκBα,[99,100]respectively. Indeed, unlike full-length NF-κB p65, nuclear import of p65 (191–308) was not stimulated by the coexpression of constitutively active IKK2 (IKK2ca), a kinase which induces phosphorylation-dependent degradation of IκBα[101] (Figure 6J). We then tested whether nuclear accumulation of p65 (191–308) could be inhibited by the TAZ NLS or the viral proteins (Figure 6K). The TAZ NLS significantly reduced import in an M-dependent way, while the viral proteins abolished it. These findings suggest that the TAZ NLS could mitigate NF-κB p65 nuclear accumulation in a signaling-independent manner. Finally, we determined whether the altered NF-κB accumulation, induced by TAZ constructs, results in a reduced transcriptional output. To this end, we measured the activity of NF-κB p65 luciferase reporter (Figures 6L and S8E). Full-length TAZ reduced TNFα-induced reporter activity, as reported earlier.[54] Surprisingly, however, the TAZ NLS failed to exert an inhibitory effect on the reporter, or even slightly elevated it. This points to the complex regulation of the system. A partial reduction in the nuclear level may not be sufficient for reduced activity, either because the TAZ NLS could stimulate the transcriptional activity of NF-κB (e.g., by antagonizing the direct effect of full-length TAZ) and/or because full-length TAZ triggers additional mechanisms (e.g., gene expression), necessary for suppression. Thus, while TAZ can reduce NF-κB nuclear import per se, the consequences of such inhibition remained to be elucidated.

DISCUSSION

The present study identifies and characterizes the M-motif (named after its critical methionine) in TAZ and YAP as an essential sequence for facilitated import into the nucleus. Definition of this molecular and functional signature then allowed us to generalize our findings in two regards; First, it suggests that the M-motif constitutes a novel class of NLS, present and functional in a variety of cellular and viral proteins; second, guided by the known actions of viral M-motifs, we discovered that TAZ/YAP are also potent inhibitors of classic nuclear import processes. This property may be a significant mechanism whereby TAZ/YAP act as endogenous suppressors of antiviral responses. These findings open new vistas both for nuclear transport and for novel and *non-transcriptional* effects of TAZ/YAP, as will be discussed below.

The M-motif, as a novel NLS for facilitated TAZ/YAP import: An integrated view

Our previous study has shown that a segment in the TAZ C-terminus is critical for its nuclear entry.[32] Here, we demonstrate that the essential attributes of the TAZ/YAP NLS include the presence of multiple negative charges flanking a methionine residue (Figure 7A). Neutralizing the charges or mutating the methionine abolishes import via this NLS. Conversely, the intact M-motif NLS is sufficient and necessary to mediate importin α/β-, Ran-, and ATP-independent facilitated diffusion across the nuclear membrane, both in isolation and in the context of the full-length molecules.

The M-motif NLS is universal in that it is present in both TAZ and YAP in an evolutionarily conserved manner (from many invertebrates to all vertebrate species), indicating its key functional significance. It is worth noting, however, that it is not found in Drosophila Yorkie (the first discovered TAZ/YAP homolog), which harbors a classic NLS within its unique N-terminus and enters the nucleus in an importin α- and Ran-dependent manner.[102] Additional differences in the molecular architecture of Yorkie are the missing transactivation domain and PBM,[103] demonstrating the divergent evolutionary fate, and thus alternative regulation, of this TAZ/YAP ortholog.

Emerging evidence supports the notion that the nuclear import of TAZ/YAP can be mediated by multiple mechanisms, which may also allow for differential regulation of the import process by various stimuli. In this regard, the PBM of YAP is critical for mechanotransduction-promoted nuclear import of YAP.[39] This sequence was found to be necessary for IPO7 binding, which in turn can shuttle YAP into the nucleus. Our findings confirm and extend the importance of the PBM, as deletion of this part significantly reduces not only the nuclear uptake of YAP, but also of TAZ. However, the M-motif NLS-mediated import is distinct from the IPO7-mediated one, since the TAZ NLS does not bind IPO7, yet it is fully import-competent. Conversely, deleting (or mutating) the M-motif fully eliminates TAZ/YAP net accumulation. Thus, the PBM and the TAZ NLS can mediate distinct import processes. Whether and how the M-motif NLS and PBM cooperate in IPO7 mediated transport is a question for future studies.

In addition to the NLS and the PBM, the WW domain has also been shown to mediate nuclear import.[36,40] Interestingly, it can also contribute to the cytosolic retention of TAZ in tubular cells.[7] In any case, these examples show that certain modes of TAZ/YAP import can be Ran- and energy-dependent (e.g., IPO7- or classic importin α/β-dependent and ivermectin sensitive). Moreover, TAZ/YAP nuclear accumulation is also determined by intranuclear retention as shown by others and us.[31,32,103] Since major nuclear retention partners (e.g., TEAD) can also cycle across the nuclear membrane,[104] altering their (often classic) import will also impact nuclear TAZ/YAP levels. These complexities were overcome by our retention- and passive diffusion-independent constructs, allowing for the identification of the novel facilitated import pathway.

The M-motif NLS-mediated import endows the entry route with specificity, but being energetically inert, it does not engender a large accumulation of intranuclear TAZ/YAP over the cytosolic level. This essential background activity is likely

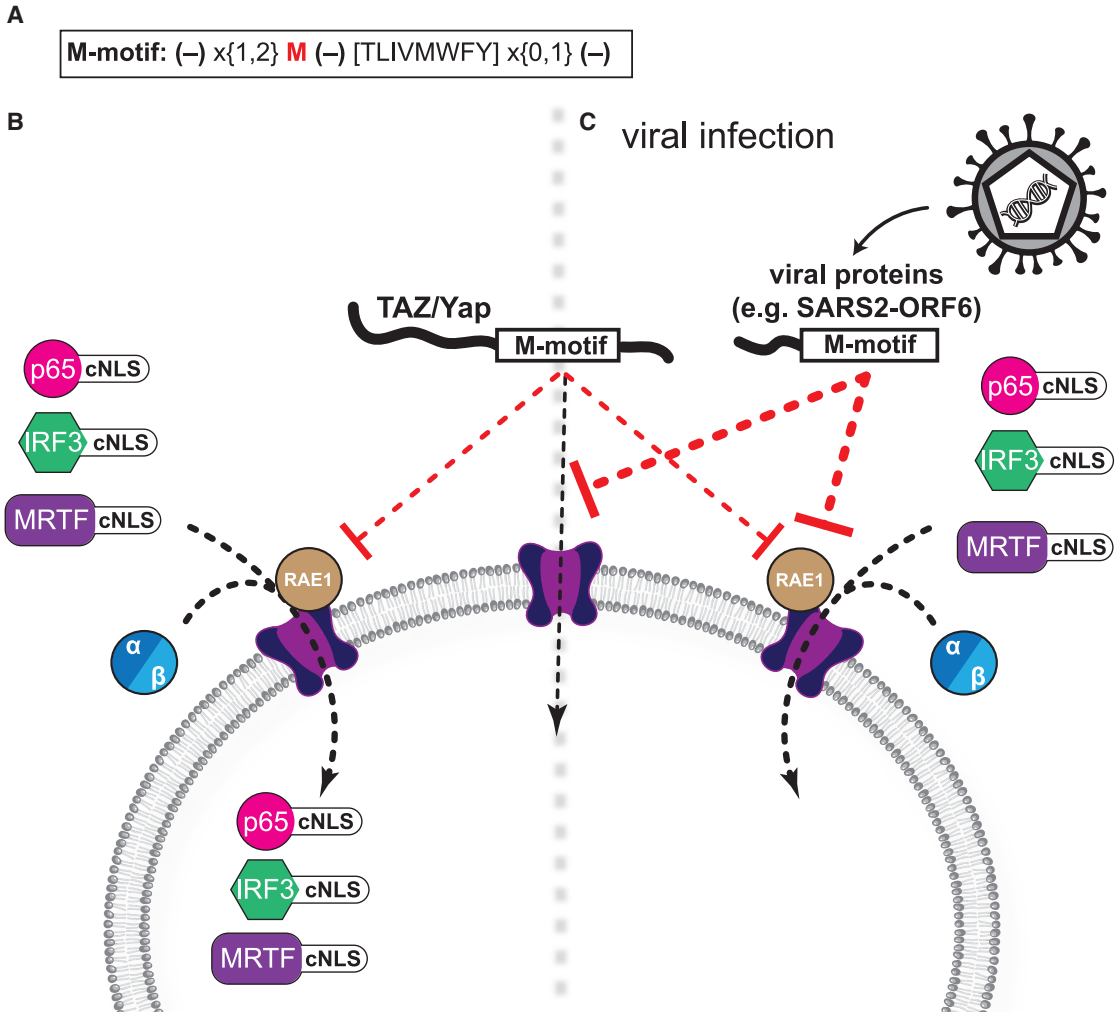

Figure 7. M-motif and model of its activities in cellular and viral proteins

(A) M-motif signature deduced from this work.

(B) The M-motif NLS of TAZ mediates TAZ import. The motif also suppresses classic protein import by directly binding to RAE1, affecting importin α/β complexes. This reduces the nuclear presence of relevant transcription factors.

(C) Viral M-motifs (e.g., in ORF6 of SARS2) suppress TAZ import presumably by competing for the same import route. Whether the viral proteins are efficiently imported themselves depends on additional localization signals and binding motifs. Viral M-motifs also supress classic protein import, mimicking the function of TAZ. Import competition between cellular M-motif NLS containing proteins is conceivable (not shown).

superimposed on other import and retention mechanisms that can lead to net nuclear TAZ/YAP accumulation. It remains to be determined whether the M-motif NLS-mediated import itself is prone to regulation by mechanical inputs. It is noteworthy that our previous data indicated that a longer segment of the TAZ C-terminus (290–345), harboring the NLS, remains responsive to RhoA stimulation.[32]

M-motif NLS in other cellular proteins – Functional implications

Based on shared import modalities and sequence similarities, this study identifies three additional cellular proteins – STAT1, cyclin B1, and hnRNPK – which contain M-motifs that mediate methionine dependent nuclear import. It is worth noting that their M-motif NLS are not the only import-promoting sequences within these proteins. Rather, they may be crucial mediators for entry under basal or specific regulatory conditions. For example, STAT1 harbors a non-conventional, signaling-dependent NLS in addition to the M-motif NLS. Interferon stimulates STAT1 tyrosine phosphorylation and dimerization, which enables binding to importin α[74] and drives STAT1 nuclear localization. We suspect that the M-motif NLS might play a crucial role in constitutive, tyrosine phosphorylation-independent shuttling and functions of STAT1.[60,75] This assumption is buttressed by the finding that people with naturally occurring M/V mutation in the STAT1 M-motif NLS[76] show increased susceptibility to mycobacterial infection. Similarly, cyclin B1 can enter the nucleus via a Ran- and importin α-independent but importin

β-dependent mechanism.[62,63] This was, however, suggested to be distinct from the phosphorylated CRS-mediated and fully importin-independent import which is critical for efficient nuclear entry of cyclin B1 at prophase, shortly preceding the dissolution of the nuclear membrane.[77,105,106] Remarkably, phosphorylation of the CRS renders it a bona fide M-motif NLS. Lastly, hnRNPK contains a classic, bipartite NLS in the N-terminus and the KNS in the C-terminal region.[64] We have shown that the M-motif NLS in the KNS is functionally important. Moreover, given that the TAZ NLS or the relevant viral proteins can mitigate TAZ entry, general competition among M-motif NLS containing proteins is conceivable. Nonetheless, the competitive nature of the inhibition remains to be proven. Irrespectively, such inhibitory mechanism may be particularly important in cancers with high levels of TAZ/YAP expression[3–5] or viral infections such as Covid-19 and warrants further investigations.

M-motif-mediated inhibition of classic import: viral homologies

A major finding of the current study is that TAZ – via its M-motif – inhibits classic protein import. We demonstrate this general effect with regards to an array of cargoes (e.g., SV40/R5A, MRTF, IRF3, and NF-κB p65), taken up via the classic (importin α/β1-mediated) pathway. Mechanistically, we show that (1) TAZ and the TAZ NLS bind RAE1, (2) RAE1 is important for classic protein import, and (3) the TAZ NLS disrupts both the RAE1/importin β1 and the cargo/importin α1/importin β1 complexes. We expect a similar function of YAP in these processes, based on sequence conservation and the reported YAP-RAE1 interaction[107] in BioGRID,[108] but this prediction necessitates further experimental validation. Insight into the underlying mechanism as well as the potential pathophysiological significance of the TAZ NLS-mediated classic import inhibition was greatly fostered by the recognition that the M-motif in TAZ shares remarkable similarity with acidic regions of various viral proteins (e.g., M-motifs in VSV-M, SARS-ORF6 and SARS2-ORF6). The sequence similarity, combined with previous evidence that (1) TAZ/YAP (via their C terminus) are endogenous suppressors of antiviral responses[53–55]; (2) viral M-motifs play a key role in such avoidance strategies (i.e., inhibition of interferon production and action)[47–52,87,88] and (3) viral M-motifs were reported to suppress protein import,[47–52,87,92,109,110] lead us to propose two important assertions (Figures 7B and 7C). (1) Mitigating classic import could be one of the mechanisms whereby TAZ/YAP exert their suppressive effect on antiviral responses. In support of this concept, the TAZ NLS inhibits the nuclear uptake of IRF3, NF-κB p65, and the "signaling-independent" p65 fragment. Regarding the abrogation of STAT1 nuclear uptake by the TAZ NLS, both classic import inhibition and competition between the respective M-motifs (see above) might play a role. (2) The implicated viruses act, in part, by hijacking a subset of the natural functions of TAZ/YAP. In support of this notion, VSV-M was shown to suppress the nuclear accumulation of NF-κB p65 and ribonucleoproteins[87,109,110] whereas ORF6 of SARS viruses mitigated nuclear localization of STAT1, IRF3 and NF-κB p65.[47–52,92] At least a part of these effects is exerted on the level of protein import itself. Indeed, these viral proteins were proposed to inhibit transport through RAE1 binding,[47,48,51,52,81,83–85] which may dismantle classic transport complexes at the Nup98-RAE1 nexus.[111–113] Finally, while viruses can exploit the classic transport-inhibitory function of TAZ/YAP, they also interfere with TAZ/YAP transport itself. In this regard, we show that SARS-Cov2 ORF6 inhibits the nuclear accumulation of TAZ/YAP, and this virus was also found to suppress cyclin B1 nuclear entry.[114] These effects may facilitate viral replication by mitigating cell proliferation and promoting cell-cycle arrest, a crucial strategy used by viruses.[115,116]

Limitations of the study

Contrary to our expectations, we found no evidence that RAE1 is necessary for the import of TAZ/YAP themselves. This is consistent with an earlier finding that RAE1 downregulation may even promote nuclear uptake of YAP, via an indirect effect on Hippo kinases.[117] Thus, the exact import mechanism for TAZ/YAP through their M-motif, or in fact for any M-motif proteins, remains an open question This would be an important step for the full characterization of this NLS. Such progress would also facilitate the assessment of the relative contributions of various import modalities to the overall TAZ/YAP uptake and their selective regulation by different inputs. In any case, the identification of this import signature, its basic molecular and functional characterization, and its fundamental role in facilitated nuclear import of TAZ/YAP and a variety of other proteins is bound to pave the road to solve this enigma. Finally, RAE1 is necessary for viral M-motifs to block nuclear mRNA export[43,80,88,91,109] as well. Accordingly, future research should address the exciting possibility that TAZ/YAP might also modulate mRNA export.

RESOURCE AVAILABILITY

Lead contact

All unique/stable reagents generated in this study are available from the Lead Contact with a completed Materials Transfer Agreement. Andras Kapus (andras.kapus@unityhealth.to).

Materials availability

This study did not generate new unique reagents apart from the listed constructs.

Data and code availability

- All data reported in this paper will be shared by the lead contact upon request.
- This paper does not report original code.
- Any additional information required to reanalyze the data reported in this paper is available from the lead contact upon request.

ACKNOWLEDGMENTS

We thank Dr. Katalin Szaszi and Dr. Kelsie Thu for the critical reading of the manuscript and for their invaluable suggestions. This work was supported by grants from Natural Sciences and Engineering Research Council of Canada (NSERC, RGPIN- 2019-05222), the Canadian Institutes of Health Research (CIHR, PJT 148608, PJT 162360) and the Kidney Foundation of Canada to A.K.

A.K. is a Thor Eaton Professor of Fibrosis Research, jointly appointed by the University of Toronto and the St. Michael's Hospital.

AUTHOR CONTRIBUTIONS

M.K. participated in the conceptualization of the project, developed the experimental approaches, generated the majority of the reagents, designed, and performed the majority of the experiments, analyzed the results, and wrote

several sections of the manuscript; S.V. performed experiments on IRF3 translocation and IFN promoter activation; G.G. participated in the in the FRAP studies; C.D.C.O. provided help with the optimization of fluorescence N/C measurements, including the setting up of new equipment; A.K. conceived the central ideas and the overall framework of the project, proposed experimental approaches, participated in data evaluation, interpretation and figure design, and wrote a substantial portion of the manuscript.

DECLARATION OF INTERESTS

The authors declare no competing interests.

STAR★METHODS

Detailed methods are provided in the online version of this paper and include the following:

- KEY RESOURCES TABLE
- EXPERIMENTAL MODEL AND STUDY PARTICIPANT DETAILS
  - Cells
- METHOD DETAILS
  - Reagents
  - Antibodies
  - Plasmid and small-interfering RNA (siRNA) transfection
  - Luciferase reporter assay
  - Immunoprecipitation and Western blotting
  - Immunofluorescence microscopy
  - FRAP experiments
  - M-motif search
- QUANTIFICATION AND STATISTICAL ANALYSIS

SUPPLEMENTAL INFORMATION

Supplemental information can be found online at https://doi.org/10.1016/j.isci.2025.112105.

Received: March 12, 2024
Revised: August 22, 2024
Accepted: February 21, 2025
Published: February 26, 2025

REFERENCES

1. Pocaterra, A., Romani, P., and Dupont, S. (2020). YAP/TAZ functions and their regulation at a glance. J. Cell Sci. *133*, jcs230425.
2. Moya, I.M., and Halder, G. (2019). Hippo-YAP/TAZ signalling in organ regeneration and regenerative medicine. Nat. Rev. Mol. Cell Biol. *20*, 211–226.
3. Zanconato, F., Cordenonsi, M., and Piccolo, S. (2019). YAP and TAZ: a signalling hub of the tumour microenvironment. Nat. Rev. Cancer *19*, 454–464.
4. Piccolo, S., Panciera, T., Contessotto, P., and Cordenonsi, M. (2023). YAP/TAZ as master regulators in cancer: modulation, function and therapeutic approaches. Nat. Cancer *4*, 9–26.
5. Franklin, J.M., Wu, Z., and Guan, K.L. (2023). Insights into recent findings and clinical application of YAP and TAZ in cancer. Nat. Rev. Cancer *23*, 512–525.
6. Liu, F., Lagares, D., Choi, K.M., Stopfer, L., Marinković, A., Vrbanac, V., Probst, C.K., Hiemer, S.E., Sisson, T.H., Horowitz, J.C., et al. (2015). Mechanosignaling through YAP and TAZ drives fibroblast activation and fibrosis. Am. J. Physiol. Lung Cell. Mol. Physiol. *308*, L344–L357.
7. Speight, P., Kofler, M., Szaszi, K., and Kapus, A. (2016). Context-dependent switch in chemo/mechanotransduction via multilevel crosstalk among cytoskeleton-regulated MRTF and TAZ and TGFbeta-regulated Smad3. Nat. Commun. *7*, 11642.
8. Dey, A., Varelas, X., and Guan, K.L. (2020). Targeting the Hippo pathway in cancer, fibrosis, wound healing and regenerative medicine. Nat. Rev. Drug Discov. *19*, 480–494.
9. Bialik, J.F., Ding, M., Speight, P., Dan, Q., Miranda, M.Z., Di Ciano-Oliveira, C., Kofler, M.M., Rotstein, O.D., Pedersen, S.F., Szászi, K., and Kapus, A. (2019). Profibrotic epithelial phenotype: a central role for MRTF and TAZ. Sci. Rep. *9*, 4323.
10. Szeto, S.G., Narimatsu, M., Lu, M., He, X., Sidiqi, A.M., Tolosa, M.F., Chan, L., De Freitas, K., Bialik, J.F., Majumder, S., et al. (2016). YAP/TAZ Are Mechanoregulators of TGF-beta-Smad Signaling and Renal Fibrogenesis. J. Am. Soc. Nephrol. *27*, 3117–3128.
11. Varelas, X., Samavarchi-Tehrani, P., Narimatsu, M., Weiss, A., Cockburn, K., Larsen, B.G., Rossant, J., and Wrana, J.L. (2010). The Crumbs complex couples cell density sensing to Hippo-dependent control of the TGF-beta-SMAD pathway. Dev. Cell *19*, 831–844.
12. Kwon, H., Kim, J., and Jho, E.H. (2022). Role of the Hippo pathway and mechanisms for controlling cellular localization of YAP/TAZ. FEBS J. *289*, 5798–5818.
13. Ma, S., Meng, Z., Chen, R., and Guan, K.L. (2019). The Hippo Pathway: Biology and Pathophysiology. Annu. Rev. Biochem. *88*, 577–604.
14. Aragona, M., Panciera, T., Manfrin, A., Giulitti, S., Michielin, F., Elvassore, N., Dupont, S., and Piccolo, S. (2013). A mechanical checkpoint controls multicellular growth through YAP/TAZ regulation by actin-processing factors. Cell *154*, 1047–1059.
15. Ahmad, U.S., Uttagomol, J., and Wan, H. (2022). The Regulation of the Hippo Pathway by Intercellular Junction Proteins. Life *12*, 1792.
16. Yu, F.X., Zhao, B., Panupinthu, N., Jewell, J.L., Lian, I., Wang, L.H., Zhao, J., Yuan, H., Tumaneng, K., Li, H., et al. (2012). Regulation of the Hippo-YAP pathway by G-protein-coupled receptor signaling. Cell *150*, 780–791.
17. Sorrentino, G., Ruggeri, N., Specchia, V., Cordenonsi, M., Mano, M., Dupont, S., Manfrin, A., Ingallina, E., Sommaggio, R., Piazza, S., et al. (2014). Metabolic control of YAP and TAZ by the mevalonate pathway. Nat. Cell Biol. *16*, 357–366.
18. Panciera, T., Azzolin, L., Cordenonsi, M., and Piccolo, S. (2017). Mechanobiology of YAP and TAZ in physiology and disease. Nat. Rev. Mol. Cell Biol. *18*, 758–770.
19. Santinon, G., Pocaterra, A., and Dupont, S. (2016). Control of YAP/TAZ Activity by Metabolic and Nutrient-Sensing Pathways. Trends Cell Biol. *26*, 289–299.
20. Dupont, S. (2016). Role of YAP/TAZ in cell-matrix adhesion-mediated signalling and mechanotransduction. Exp. Cell Res. *343*, 42–53.
21. Halder, G., Dupont, S., and Piccolo, S. (2012). Transduction of mechanical and cytoskeletal cues by YAP and TAZ. Nat. Rev. Mol. Cell Biol. *13*, 591–600.
22. Cai, X., Wang, K.C., and Meng, Z. (2021). Mechanoregulation of YAP and TAZ in Cellular Homeostasis and Disease Progression. Front. Cell Dev. Biol. *9*, 673599.
23. Zhao, B., Li, L., Tumaneng, K., Wang, C.Y., and Guan, K.L. (2010). A coordinated phosphorylation by Lats and CK1 regulates YAP stability through SCF(beta-TRCP). Genes Dev. *24*, 72–85.
24. Miranda, M.Z., Bialik, J.F., Speight, P., Dan, Q., Yeung, T., Szászi, K., Pedersen, S.F., and Kapus, A. (2017). TGF-beta1 regulates the expression and transcriptional activity of TAZ protein via a Smad3-independent, myocardin-related transcription factor-mediated mechanism. J. Biol. Chem. *292*, 14902–14920.
25. Zhao, B., Wei, X., Li, W., Udan, R.S., Yang, Q., Kim, J., Xie, J., Ikenoue, T., Yu, J., Li, L., et al. (2007). Inactivation of YAP oncoprotein by the Hippo pathway is involved in cell contact inhibition and tissue growth control. Genes Dev. *21*, 2747–2761.
26. Freeman, A.K., and Morrison, D.K. (2011). 14-3-3 Proteins: diverse functions in cell proliferation and cancer progression. Semin. Cell Dev. Biol. *22*, 681–687.

27. Mana-Capelli, S., Paramasivam, M., Dutta, S., and McCollum, D. (2014). Angiomotins link F-actin architecture to Hippo pathway signaling. Mol. Biol. Cell *25*, 1676–1685.

28. Dasgupta, I., and McCollum, D. (2019). Control of cellular responses to mechanical cues through YAP/TAZ regulation. J. Biol. Chem. *294*, 17693–17706.

29. Zhao, B., Ye, X., Yu, J., Li, L., Li, W., Li, S., Yu, J., Lin, J.D., Wang, C.Y., Chinnaiyan, A.M., et al. (2008). TEAD mediates YAP-dependent gene induction and growth control. Genes Dev. *22*, 1962–1971.

30. Zhang, H., Liu, C.Y., Zha, Z.Y., Zhao, B., Yao, J., Zhao, S., Xiong, Y., Lei, Q.Y., and Guan, K.L. (2009). TEAD transcription factors mediate the function of TAZ in cell growth and epithelial-mesenchymal transition. J. Biol. Chem. *284*, 13355–13362.

31. Chan, S.W., Lim, C.J., Loo, L.S., Chong, Y.F., Huang, C., and Hong, W. (2009). TEADs mediate nuclear retention of TAZ to promote oncogenic transformation. J. Biol. Chem. *284*, 14347–14358.

32. Kofler, M., Speight, P., Little, D., Di Ciano-Oliveira, C., Szászi, K., and Kapus, A. (2018). Mediated nuclear import and export of TAZ and the underlying molecular requirements. Nat. Commun. *9*, 4966.

33. Manning, S.A., Dent, L.G., Kondo, S., Zhao, Z.W., Plachta, N., and Harvey, K.F. (2018). Dynamic Fluctuations in Subcellular Localization of the Hippo Pathway Effector Yorkie In Vivo. Curr. Biol. *28*, 1651–1660.e4.

34. Kanai, F., Marignani, P.A., Sarbassova, D., Yagi, R., Hall, R.A., Donowitz, M., Hisaminato, A., Fujiwara, T., Ito, Y., Cantley, L.C., and Yaffe, M.B. (2000). TAZ: a novel transcriptional co-activator regulated by interactions with 14-3-3 and PDZ domain proteins. EMBO J. *19*, 6778–6791.

35. Kofler, M., and Kapus, A. (2023). Nuclear Import and Export of YAP and TAZ. Cancers *15*, 4956.

36. Kim, J., Kwon, H., Shin, Y.K., Song, G., Lee, T., Kim, Y., Jeong, W., Lee, U., Zhang, X., Nam, G., et al. (2020). MAML1/2 promote YAP/TAZ nuclear localization and tumorigenesis. Proc. Natl. Acad. Sci. USA *117*, 13529–13540.

37. Sidor, C., Borreguero-Munoz, N., Fletcher, G.C., Elbediwy, A., Guillermin, O., and Thompson, B.J. (2019). Mask family proteins ANKHD1 and ANKRD17 regulate YAP nuclear import and stability. Elife *8*, e48601.

38. Nagashima, S., Maruyama, J., Honda, K., Kondoh, Y., Osada, H., Nawa, M., Nakahama, K.I., Ishigami-Yuasa, M., Kagechika, H., Sugimura, H., et al. (2021). CSE1L promotes nuclear accumulation of transcriptional coactivator TAZ and enhances invasiveness of human cancer cells. J. Biol. Chem. *297*, 100803.

39. García-García, M., Sánchez-Perales, S., Jarabo, P., Calvo, E., Huyton, T., Fu, L., Ng, S.C., Sotodosos-Alonso, L., Vázquez, J., Casas-Tintó, S., and Görlich, D. (2022). Mechanical control of nuclear import by Importin-7 is regulated by its dominant cargo YAP. Nat. Commun. *13*, 1174.

40. Yang, Y., Wu, M., Pan, Y., Hua, Y., He, X., Li, X., Wang, J., and Gan, X. (2024). WW domains form a folded type of nuclear localization signal to guide YAP1 nuclear import. J. Cell Biol. *223*, e202308013.

41. Ege, N., Dowbaj, A.M., Jiang, M., Howell, M., Hooper, S., Foster, C., Jenkins, R.P., and Sahai, E. (2018). Quantitative Analysis Reveals that Actin and Src-Family Kinases Regulate Nuclear YAP1 and Its Export. Cell Syst. *6*, 692–708.e13.

42. Furukawa, K.T., Yamashita, K., Sakurai, N., and Ohno, S. (2017). The Epithelial Circumferential Actin Belt Regulates YAP/TAZ through Nucleocytoplasmic Shuttling of Merlin. Cell Rep. *20*, 1435–1447.

43. Gong, D., Kim, Y.H., Xiao, Y., Du, Y., Xie, Y., Lee, K.K., Feng, J., Farhat, N., Zhao, D., Shu, S., et al. (2016). A Herpesvirus Protein Selectively Inhibits Cellular mRNA Nuclear Export. Cell Host Microbe *20*, 642–653.

44. Petersen, J.M., Her, L.S., and Dahlberg, J.E. (2001). Multiple vesiculoviral matrix proteins inhibit both nuclear export and import. Proc. Natl. Acad. Sci. USA *98*, 8590–8595.

45. Petersen, J.M., Her, L.S., Varvel, V., Lund, E., and Dahlberg, J.E. (2000). The matrix protein of vesicular stomatitis virus inhibits nucleocytoplasmic transport when it is in the nucleus and associated with nuclear pore complexes. Mol. Cell Biol. *20*, 8590–8601.

46. Hussain, S., and Gallagher, T. (2010). SARS-coronavirus protein 6 conformations required to impede protein import into the nucleus. Virus Res. *153*, 299–304.

47. Miorin, L., Kehrer, T., Sanchez-Aparicio, M.T., Zhang, K., Cohen, P., Patel, R.S., Cupic, A., Makio, T., Mei, M., Moreno, E., et al. (2020). SARS-CoV-2 Orf6 hijacks Nup98 to block STAT nuclear import and antagonize interferon signaling. Proc. Natl. Acad. Sci. USA *117*, 28344–28354.

48. Addetia, A., Lieberman, N.A.P., Phung, Q., Hsiang, T.Y., Xie, H., Roychoudhury, P., Shrestha, L., Loprieno, M.A., Huang, M.L., Gale, M., Jr., et al. (2021). SARS-CoV-2 ORF6 Disrupts Bidirectional Nucleocytoplasmic Transport through Interactions with Rae1 and Nup98. MBio *12*, 10–1128.

49. Wong, H.T., Cheung, V., and Salamango, D.J. (2022). Decoupling SARS-CoV-2 ORF6 localization and interferon antagonism. J. Cell Sci. *135*, jcs259666.

50. Miyamoto, Y., Itoh, Y., Suzuki, T., Tanaka, T., Sakai, Y., Koido, M., Hata, C., Wang, C.X., Otani, M., Moriishi, K., et al. (2022). SARS-CoV-2 ORF6 disrupts nucleocytoplasmic trafficking to advance viral replication. Commun. Biol. *5*, 483.

51. Kimura, I., Konno, Y., Uriu, K., Hopfensperger, K., Sauter, D., Nakagawa, S., and Sato, K. (2021). Sarbecovirus ORF6 proteins hamper induction of interferon signaling. Cell Rep. *34*, 108916.

52. Lei, X., Dong, X., Ma, R., Wang, W., Xiao, X., Tian, Z., Wang, C., Wang, Y., Li, L., Ren, L., et al. (2020). Activation and evasion of type I interferon responses by SARS-CoV-2. Nat. Commun. *11*, 3810.

53. Zhang, Q., Meng, F., Chen, S., Plouffe, S.W., Wu, S., Liu, S., Li, X., Zhou, R., Wang, J., Zhao, B., et al. (2017). Hippo signalling governs cytosolic nucleic acid sensing through YAP/TAZ-mediated TBK1 blockade. Nat. Cell Biol. *19*, 362–374.

54. Deng, Y., Lu, J., Li, W., Wu, A., Zhang, X., Tong, W., Ho, K.K., Qin, L., Song, H., and Mak, K.K. (2018). Reciprocal inhibition of YAP/TAZ and NF-kappaB regulates osteoarthritic cartilage degradation. Nat. Commun. *9*, 4564.

55. Wang, S., Xie, F., Chu, F., Zhang, Z., Yang, B., Dai, T., Gao, L., Wang, L., Ling, L., Jia, J., et al. (2017). YAP antagonizes innate antiviral immunity and is targeted for lysosomal degradation through IKKvarepsilon-mediated phosphorylation. Nat. Immunol. *18*, 733–743.

56. Kofler, M., and Kapus, A. (2021). Nucleocytoplasmic Shuttling of the Mechanosensitive Transcription Factors MRTF and YAP/TAZ. Methods Mol. Biol. *2299*, 197–216.

57. Fan, L., Sebe, A., Péterfi, Z., Masszi, A., Thirone, A.C.P., Rotstein, O.D., Nakano, H., McCulloch, C.A., Szászi, K., Mucsi, I., and Kapus, A. (2007). Cell contact-dependent regulation of epithelial-myofibroblast transition via the rho-rho kinase-phospho-myosin pathway. Mol. Biol. Cell *18*, 1083–1097.

58. Masszi, A., Speight, P., Charbonney, E., Lodyga, M., Nakano, H., Szászi, K., and Kapus, A. (2010). Fate-determining mechanisms in epithelial-myofibroblast transition: major inhibitory role for Smad3. J. Cell Biol. *188*, 383–399.

59. Schwoebel, E.D., Ho, T.H., and Moore, M.S. (2002). The mechanism of inhibition of Ran-dependent nuclear transport by cellular ATP depletion. J. Cell Biol. *157*, 963–974.

60. Meyer, T., Begitt, A., Lödige, I., van Rossum, M., and Vinkemeier, U. (2002). Constitutive and IFN-gamma-induced nuclear import of STAT1 proceed through independent pathways. EMBO J. *21*, 344–354.

61. Marg, A., Shan, Y., Meyer, T., Meissner, T., Brandenburg, M., and Vinkemeier, U. (2004). Nucleocytoplasmic shuttling by nucleoporins Nup153 and Nup214 and CRM1-dependent nuclear export control the subcellular distribution of latent Stat1. J. Cell Biol. *165*, 823–833.

62. Moore, J.D., Yang, J., Truant, R., and Kornbluth, S. (1999). Nuclear import of Cdk/cyclin complexes: identification of distinct mechanisms

for import of Cdk2/cyclin E and Cdc2/cyclin B1. J. Cell Biol. *144*, 213–224.

63. Takizawa, C.G., Weis, K., and Morgan, D.O. (1999). Ran-independent nuclear import of cyclin B1-Cdc2 by importin beta. Proc. Natl. Acad. Sci. USA *96*, 7938–7943.
64. Michael, W.M., Eder, P.S., and Dreyfuss, G. (1997). The K nuclear shuttling domain: a novel signal for nuclear import and nuclear export in the hnRNP K protein. EMBO J. *16*, 3587–3598.
65. Stark, G.R., and Darnell, J.E., Jr. (2012). The JAK-STAT pathway at twenty. Immunity *36*, 503–514.
66. Lindqvist, A., Rodríguez-Bravo, V., and Medema, R.H. (2009). The decision to enter mitosis: feedback and redundancy in the mitotic entry network. J. Cell Biol. *185*, 193–202.
67. Takizawa, C.G., and Morgan, D.O. (2000). Control of mitosis by changes in the subcellular location of cyclin-B1-Cdk1 and Cdc25C. Curr. Opin. Cell Biol. *12*, 658–665.
68. Strauss, B., Harrison, A., Coelho, P.A., Yata, K., Zernicka-Goetz, M., and Pines, J. (2018). Cyclin B1 is essential for mitosis in mouse embryos, and its nuclear export sets the time for mitosis. J. Cell Biol. *217*, 179–193.
69. Pinol-Roma, S., and Dreyfuss, G. (1993). hnRNP proteins: localization and transport between the nucleus and the cytoplasm. Trends Cell Biol. *3*, 151–155.
70. Chan, J.Y.H., Huang, S.M., Liu, S.T., and Huang, C.H. (2008). The transactivation domain of heterogeneous nuclear ribonucleoprotein K overlaps its nuclear shuttling domain. Int. J. Biochem. Cell Biol. *40*, 2078–2089.
71. Xia, A., Yuan, W., Wang, Q., Xu, J., Gu, Y., Zhang, L., Chen, C., Wang, Z., Wu, D., He, Q., et al. (2022). The cancer-testis lncRNA lnc-CTHCC promotes hepatocellular carcinogenesis by binding hnRNP K and activating YAP1 transcription. Nat. Cancer *3*, 203–218.
72. Levy, D.E., and Darnell, J.E., Jr. (2002). Stats: transcriptional control and biological impact. Nat. Rev. Mol. Cell Biol. *3*, 651–662.
73. Awasthi, N., Liongue, C., and Ward, A.C. (2021). STAT proteins: a kaleidoscope of canonical and non-canonical functions in immunity and cancer. J. Hematol. Oncol. *14*, 198.
74. McBride, K.M., Banninger, G., McDonald, C., and Reich, N.C. (2002). Regulated nuclear import of the STAT1 transcription factor by direct binding of importin-alpha. EMBO J. *21*, 1754–1763.
75. Cheon, H., and Stark, G.R. (2009). Unphosphorylated STAT1 prolongs the expression of interferon-induced immune regulatory genes. Proc. Natl. Acad. Sci. USA *106*, 9373–9378.
76. Liu, Z., Zhou, M., Yuan, C., Ni, Z., Liu, W., Tan, Y., Zhang, D., Zhou, X., Zou, T., Wang, J., et al. (2022). Two novel STAT1 mutations cause Mendelian susceptibility to mycobacterial disease. Biochem. Biophys. Res. Commun. *591*, 124–129.
77. Hagting, A., Jackman, M., Simpson, K., and Pines, J. (1999). Translocation of cyclin B1 to the nucleus at prophase requires a phosphorylation-dependent nuclear import signal. Curr. Biol. *9*, 680–689.
78. Pines, J., and Hunter, T. (1994). The differential localization of human cyclins A and B is due to a cytoplasmic retention signal in cyclin B. EMBO J. *13*, 3772–3781.
79. Yang, J., Bardes, E.S., Moore, J.D., Brennan, J., Powers, M.A., and Kornbluth, S. (1998). Control of cyclin B1 localization through regulated binding of the nuclear export factor CRM1. Genes Dev. *12*, 2131–2143.
80. Feng, H., Tian, H., Wang, Y., Zhang, Q., Lin, N., Liu, S., Yu, Y., Deng, H., and Gao, P. (2020). Molecular mechanism underlying selective inhibition of mRNA nuclear export by herpesvirus protein ORF10. Proc. Natl. Acad. Sci. USA *117*, 26719–26727.
81. Li, T., Wen, Y., Guo, H., Yang, T., Yang, H., and Ji, X. (2021). Molecular Mechanism of SARS-CoVs Orf6 Targeting the Rae1-Nup98 Complex to Compete With mRNA Nuclear Export. Front. Mol. Biosci. *8*, 813248.
82. Quan, B., Seo, H.S., Blobel, G., and Ren, Y. (2014). Vesiculoviral matrix (M) protein occupies nucleic acid binding site at nucleoporin pair (Rae1 * Nup98). Proc. Natl. Acad. Sci. USA *111*, 9127–9132.
83. Gao, X., Tian, H., Zhu, K., Li, Q., Hao, W., Wang, L., Qin, B., Deng, H., and Cui, S. (2022). Structural basis for Sarbecovirus ORF6 mediated blockage of nucleocytoplasmic transport. Nat. Commun. *13*, 4782.
84. Gordon, D.E., Jang, G.M., Bouhaddou, M., Xu, J., Obernier, K., White, K.M., O'Meara, M.J., Rezelj, V.V., Guo, J.Z., Swaney, D.L., et al. (2020). A SARS-CoV-2 protein interaction map reveals targets for drug repurposing. Nature *583*, 459–468.
85. Kato, K., Ikliptikawati, D.K., Kobayashi, A., Kondo, H., Lim, K., Hazawa, M., and Wong, R.W. (2021). Overexpression of SARS-CoV-2 protein ORF6 dislocates RAE1 and NUP98 from the nuclear pore complex. Biochem. Biophys. Res. Commun. *536*, 59–66.
86. Yoo, T.Y., and Mitchison, T. (2022). Quantification of nuclear transport inhibition by SARS-CoV-2 ORF6 using a broadly applicable live-cell dose-response pipeline. Preprint at bioRxiv. https://doi.org/10.1101/2021.12.10.472151.
87. Varble, A.J., Ried, C.D., Hammond, W.J., Marquis, K.A., Woodruff, M.C., and Ferran, M.C. (2016). The vesicular stomatitis virus matrix protein inhibits NF-kappaB activation in mouse L929 cells. Virology *499*, 99–104.
88. Hall, R., Guedán, A., Yap, M.W., Young, G.R., Harvey, R., Stoye, J.P., and Bishop, K.N. (2022). SARS-CoV-2 ORF6 disrupts innate immune signalling by inhibiting cellular mRNA export. PLoS Pathog. *18*, e1010349.
89. von Kobbe, C., van Deursen, J.M., Rodrigues, J.P., Sitterlin, D., Bachi, A., Wu, X., Wilm, M., Carmo-Fonseca, M., and Izaurralde, E. (2000). Vesicular stomatitis virus matrix protein inhibits host cell gene expression by targeting the nucleoporin Nup98. Mol. Cell *6*, 1243–1252.
90. Her, L.S., Lund, E., and Dahlberg, J.E. (1997). Inhibition of Ran guanosine triphosphatase-dependent nuclear transport by the matrix protein of vesicular stomatitis virus. Science *276*, 1845–1848.
91. Faria, P.A., Chakraborty, P., Levay, A., Barber, G.N., Ezelle, H.J., Enninga, J., Arana, C., van Deursen, J., and Fontoura, B.M.A. (2005). VSV disrupts the Rae1/mrnp41 mRNA nuclear export pathway. Mol. Cell *17*, 93–102.
92. Xia, H., Cao, Z., Xie, X., Zhang, X., Chen, J.Y.C., Wang, H., Menachery, V.D., Rajsbaum, R., and Shi, P.Y. (2020). Evasion of Type I Interferon by SARS-CoV-2. Cell Rep. *33*, 108234.
93. Frieman, M., Yount, B., Heise, M., Kopecky-Bromberg, S.A., Palese, P., and Baric, R.S. (2007). Severe acute respiratory syndrome coronavirus ORF6 antagonizes STAT1 function by sequestering nuclear import factors on the rough endoplasmic reticulum/Golgi membrane. J. Virol. *81*, 9812–9824.
94. Makio, T., Zhang, K., Love, N., Mast, F.D., Liu, X., Elaish, M., Hobman, T., Aitchison, J.D., Fontoura, B.M.A., and Wozniak, R.W. (2024). SARS-CoV-2 Orf6 is positioned in the nuclear pore complex by Rae1 to inhibit nucleocytoplasmic transport. Mol. Biol. Cell *35*, ar62.
95. Blower, M.D., Nachury, M., Heald, R., and Weis, K. (2005). A Rae1-containing ribonucleoprotein complex is required for mitotic spindle assembly. Cell *121*, 223–234.
96. Yoo, T.Y., and Mitchison, T.J. (2024). Quantitative comparison of nuclear transport inhibition by SARS coronavirus ORF6 reveals the importance of oligomerization. Proc. Natl. Acad. Sci. USA *121*, e2307997121.
97. Fagerlund, R., Kinnunen, L., Kohler, M., Julkunen, I., and Melen, K. (2005). NF-kappaB is transported into the nucleus by importin alpha3 and importin alpha4. J. Biol. Chem. *280*, 15942–15951.
98. Hayden, M.S., and Ghosh, S. (2014). Regulation of NF-kappaB by TNF family cytokines. Semin. Immunol. *26*, 253–266.
99. Bergqvist, S., Croy, C.H., Kjaergaard, M., Huxford, T., Ghosh, G., and Komives, E.A. (2006). Thermodynamics reveal that helix four in the NLS of NF-kappaB p65 anchors IkappaBalpha, forming a very stable complex. J. Mol. Biol. *360*, 421–434.

100. Huxford, T., and Ghosh, G. (2009). A structural guide to proteins of the NF-kappaB signaling module. Cold Spring Harb. Perspect. Biol. *1*, a000075.

101. Mercurio, F., Zhu, H., Murray, B.W., Shevchenko, A., Bennett, B.L., Li, J., Young, D.B., Barbosa, M., Mann, M., Manning, A., and Rao, A. (1997). IKK-1 and IKK-2: cytokine-activated IkappaB kinases essential for NF-kappaB activation. Science *278*, 860–866.

102. Wang, S., Lu, Y., Yin, M.X., Wang, C., Wu, W., Li, J., Wu, W., Ge, L., Hu, L., Zhao, Y., and Zhang, L. (2016). Importin alpha1 Mediates Yorkie Nuclear Import via an N-terminal Non-canonical Nuclear Localization Signal. J. Biol. Chem. *291*, 7926–7937.

103. Manning, S.A., Kroeger, B., and Harvey, K.F. (2020). The regulation of Yorkie, YAP and TAZ: new insights into the Hippo pathway. Development *147*, dev179069.

104. Magico, A.C., and Bell, J.B. (2011). Identification of a classical bipartite nuclear localization signal in the Drosophila TEA/ATTS protein scalloped. PLoS One *6*, e21431.

105. Pines, J., and Hunter, T. (1991). Human cyclins A and B1 are differentially located in the cell and undergo cell cycle-dependent nuclear transport. J. Cell Biol. *115*, 1–17.

106. Gavet, O., and Pines, J. (2010). Activation of cyclin B1-Cdk1 synchronizes events in the nucleus and the cytoplasm at mitosis. J. Cell Biol. *189*, 247–259.

107. Couzens, A.L., Knight, J.D.R., Kean, M.J., Teo, G., Weiss, A., Dunham, W.H., Lin, Z.Y., Bagshaw, R.D., Sicheri, F., Pawson, T., et al. (2013). Protein interaction network of the mammalian Hippo pathway reveals mechanisms of kinase-phosphatase interactions. Sci. Signal. *6*, rs15.

108. Oughtred, R., Rust, J., Chang, C., Breitkreutz, B.J., Stark, C., Willems, A., Boucher, L., Leung, G., Kolas, N., Zhang, F., et al. (2021). The BioGRID database: A comprehensive biomedical resource of curated protein, genetic, and chemical interactions. Protein Sci. *30*, 187–200.

109. Pettit Kneller, E.L., Connor, J.H., and Lyles, D.S. (2009). hnRNPs Relocalize to the cytoplasm following infection with vesicular stomatitis virus. J. Virol. *83*, 770–780.

110. Redondo, N., Madan, V., Alvarez, E., and Carrasco, L. (2015). Impact of Vesicular Stomatitis Virus M Proteins on Different Cellular Functions. PLoS One *10*, e0131137.

111. Wu, X., Kasper, L.H., Mantcheva, R.T., Mantchev, G.T., Springett, M.J., and van Deursen, J.M. (2001). Disruption of the FG nucleoporin NUP98 causes selective changes in nuclear pore complex stoichiometry and function. Proc. Natl. Acad. Sci. USA *98*, 3191–3196.

112. Schmidt, H.B., and Gorlich, D. (2015). Nup98 FG domains from diverse species spontaneously phase-separate into particles with nuclear pore-like permselectivity. Elife *4*, e04251.

113. Bayliss, R., Littlewood, T., and Stewart, M. (2000). Structural basis for the interaction between FxFG nucleoporin repeats and importin-beta in nuclear trafficking. Cell *102*, 99–108.

114. Sui, L., Li, L., Zhao, Y., Zhao, Y., Hao, P., Guo, X., Wang, W., Wang, G., Li, C., and Liu, Q. (2023). Host cell cycle checkpoint as antiviral target for SARS-CoV-2 revealed by integrative transcriptome and proteome analyses. Signal Transduct. Target. Ther. *8*, 21.

115. Su, M., Chen, Y., Qi, S., Shi, D., Feng, L., and Sun, D. (2020). A Mini-Review on Cell Cycle Regulation of Coronavirus Infection. Front. Vet. Sci. *7*, 586826.

116. Bressy, C., Droby, G.N., Maldonado, B.D., Steuerwald, N., and Grdzelishvili, V.Z. (2019). Cell Cycle Arrest in G(2)/M Phase Enhances Replication of Interferon-Sensitive Cytoplasmic RNA Viruses via Inhibition of Antiviral Gene Expression. J. Virol. *93*, e01885-18.

117. Jahanshahi, M., Hsiao, K., Jenny, A., and Pfleger, C.M. (2016). The Hippo Pathway Targets Rae1 to Regulate Mitosis and Organ Size and to Feed Back to Regulate Upstream Components Merlin, Hippo, and Warts. PLoS Genet. *12*, e1006198.

118. Pearson, J.D., Huang, K., Pacal, M., McCurdy, S.R., Lu, S., Aubry, A., Yu, T., Wadosky, K.M., Zhang, L., Wang, T., et al. (2021). Binary pan-cancer classes with distinct vulnerabilities defined by pro- or anti-cancer YAP/TEAD activity. Cancer Cell *39*, 1115–1134.e12.

119. Krystkowiak, I., and Davey, N.E. (2017). SLiMSearch: a framework for proteome-wide discovery and annotation of functional modules in intrinsically disordered regions. Nucleic Acids Res. *45*, W464–W469.

120. Chen, L., Fischle, W., Verdin, E., and Greene, W.C. (2001). Duration of nuclear NF-kappaB action regulated by reversible acetylation. Science *293*, 1653–1657.

121. Stirling, D.R., Swain-Bowden, M.J., Lucas, A.M., Carpenter, A.E., Cimini, B.A., and Goodman, A. (2021). CellProfiler 4: improvements in speed, utility and usability. BMC Bioinformatics *22*, 433.

STAR★METHODS

KEY RESOURCES TABLE

REAGENT or RESOURCE	SOURCE	IDENTIFIER
Antibodies		
Rabbit anti-GFP	Santa Cruz Biotechnology	Cat# SC-8334, RRID: AB_641123
Mouse anti-IPO7	Santa Cruz Biotechnology	Cat# SC-365231; RRID:N/A
Mouse anti-KPNA2	Santa Cruz Biotechnology	Cat# SC-55538; RRID:AB_831493
Mouse anti-KPNB1	Santa Cruz Biotechnology	Cat# SC-137016; RRID:N/A
Mouse anti-RAE1	Santa Cruz Biotechnology	Cat# SC-393252; RRID:N/A
Mouse anti-DsRed	Santa Cruz Biotechnology	Cat# SC-390909; RRID: AB_2801575
Rabbit anti-GFP	Cell Signaling Technology	Cat# 2555; RRID:AB_10692764
Rabbit anti-tubulin	Cell Signaling Technology	Cat# 2128; RRID:AB_823664
Rabbit anti-YAP/TAZ	Cell Signaling Technology	Cat# 8418; RRID:AB_10950494
Rabbit anti-IRF3	Cell Signaling Technology	Cat# 4302; RRID: RRID:AB_1904036
Rabbit anti-MRTF	Cell Signaling Technology	Cat# 97109; RRID:N/A
Mouse anti-p65	Santa Cruz Biotechnology	Cat# SC-8008; RRID: AB_628017
Mouse anti-TAZ	BD Biosciences	Cat# 560235; RRID:AB_1645338
Mouse anti-Myc	Thermo Fisher Scientific	Cat #AHO0062; RRID:AB_2536303
Chemicals, peptides, and recombinant proteins		
Jetprime transfection reagent	Polyplus transfection	Cat# 114-07
Recombinant human TNFα	Abcam	Cat# ab9642
Leptomycin B	Sigma-Aldrich	Cat# L2913, CAS 87081-35-4
Rapamycin	Sigma-Aldrich	Cat# 553211
poly(I:C)	Sigma-Aldrich	Cat# P1530, CAS 42424-50-0
Ivermectin	Sigma-Aldrich	Cat# I8898, CAS 70288-86-7
Critical commercial assays		
Dual luciferase Reporter assay	Promega	Cat# E1910
Experimental models: Cell lines		
LLCPK1 – Kidney tubular epithelial cell line	Gift - R.C. Harris, Vanderbilt University School of Medicine	
hTERT-RPE	ATCC	Cat# CRL-4000, RRID:CVCL_4388
HEK 293T, a human epithelial-like embryonic kidney cell line	Gift – G. Gupta, Toronto Metropolitan University	Cat# CRL-3216, RRID:CVCL_0063
Oligonucleotides		
Control Non-related (NR) siRNA	Applied Biosystems	AM4635
siRNA TAZ 5′-CAAGAACATACACCTACGGTTGT-3′	Thermo Scientific/Sigma-Aldrich	Sus scrofa
siRNA YAP 5′-TCAAAGCGCTCCAGTGAAA-3′	Thermo Scientific/Sigma-Aldrich	Sus scrofa
siRNA RAE1 5′- GGACAAAGATGCCAGAACA-3	Thermo Scientific/Sigma-Aldrich	Sus scrofa
siRNA RAN 5′-GCAACAAAGTGGATATTAA-3′	Thermo Scientific/Sigma-Aldrich	Sus scrofa
Recombinant DNA		
pGL3-INFβ-luc or pGL4.32[luc2P/NF-κB-RE/Hygro]	Promega	E8491
pRL-Renilla Luciferase-TK control reporter vector	Promega	E224A
IKK-2 S177E S181E	Addgene	Plasmid #11105; RRID:Addgene_11105
pcDNA-GFP-STAT1	Addgene	Plasmid #11987; RRID:Addgene_11987
pCAG-VSVM	Addgene	Plasmid #64086; RRID:Addgene_64086
GFP-RelA	Addgene	Plasmid #23255; RRID:Addgene_23255
RVFV-NSs	Sino Biological	CAS# VG40339-G; RRID:N/A
YAP 5SA	Gift: Jeff Wrana	Pearson et al.[118]

(*Continued on next page*)

Continued

REAGENT or RESOURCE	SOURCE	IDENTIFIER
pGL3-INFβ-luc	Gift: John Hiscott and Marc Servant	
pcDNA3.1(-)mCherry	Kofler et al.[32]	N/A
pcDNA3.1(-)mCitrine	Kofler et al.[32]	N/A
pcDNA3.1(-)3mCitrine	Kofler et al.[32]	N/A
pcDNA3.1(-)5mCitrine	Kofler et al.[32]	N/A
pcDNA3.1(-)mCitrine-TAZ 4SA	Kofler et al.[32]	N/A
pcDNA3.1(-)mCitrine-TAZ	Kofler et al.[32]	N/A
pcDNA3.1(-)5mCitrine-TAZ 4SA	Kofler et al.[32]	N/A
pcDNA3.1(-)5mCitrine-TAZ (327-341 = NLS)	Kofler et al.[32]	N/A
pcDNA3.1(-)5mCitrine-R5A	Kofler et al.[32]	N/A
pcDNA3.1(-)5mCitrine SV40 NLS	Kofler et al.[32]	N/A
pcDNA3.1(-)5C-FRB	Kofler et al.[32]	N/A
pcDNA3.1(-)5C-FRB-TAZ(290-345)	Kofler et al.[32]	N/A
pcDNA3.1(-)H2B-2xFKBP-mCherry	Kofler et al.[32]	N/A
pcDNA3.1(-)5mCitrine-R5A-NES	This work	N/A
pcDNA3.1(-)5mCitrine-TAZ 4SA M337V	This work	N/A
pcDNA3.1(-)5mCitrine-TAZ 4SA ΔPBM	This work	N/A
pcDNA3.1(-)5mCitrine-TAZ 4SA ΔNLS	This work	N/A
pcDNA3.1(-)5mCitrine-TAZ 4SA Δ321-332	This work	N/A
pcDNA3.1(-)5mCitrine-TAZ 4SA Δ3FLxxΦ	This work	N/A
pcDNA3.1(-)5mCitrine-TAZ 4SA Δ333-345	This work	N/A
pcDNA3.1(-)5mCitrine-TAZ 4SA D338A/E341A	This work	N/A
pcDNA3.1(-)mCitrine-TAZ 4SA M337V	This work	N/A
pcDNA3.1(-)mCitrine-TAZ 4SA ΔPBM	This work	N/A
pcDNA3.1(-)mCitrine-TAZ 4SA ΔNLS	This work	N/A
pcDNA3.1(-)mCitrine-TAZ 4SA neutral	This work	N/A
pcDNA3.1(-)mCitrine-TAZ 4SA Δ3FLxxΦ	This work	N/A
pcDNA3.1(-)mCitrine-TAZ 4SA D338A/E341A	This work	N/A
pcDNA3.1(-)5mCitrine-YAP 5SA	This work	N/A
pcDNA3.1(-)5mCitrine-YAP 5SA ΔPBM	This work	N/A
pcDNA3.1(-)5mCitrine-YAP 5SA ΔNLS	This work	N/A
pcDNA3.1(-)mCitrine-TAZ NLS	This work	N/A
pcDNA3.1(-)mCitrine-TAZ NLS M337V	This work	N/A
pcDNA3.1(-)mCherry-TAZ NLS	This work	N/A
pcDNA3.1(-)mCherry-TAZ NLS M337V	This work	N/A
pcDNA3.1(-)mCherry-TAZ NLS E328A|D329A	This work	N/A
pcDNA3.1(-)mCherry-TAZ NLS D335A|E336A	This work	N/A
pcDNA3.1(-)mCherry-TAZ NLS D338A|E341A	This work	N/A
pcDNA3.1(-)5mCitrine-TAZ NLS point mutants	This work	N/A
pcDNA3.1(-)5mCitrine-YAP NLS	This work	N/A
pcDNA3.1(-)3mCitrine-TAZ NLS	This work	N/A
pcDNA3.1(-)3mCitrine-TAZ NLS M337V	This work	N/A
pcDNA3.1(-)5mCitrine-STAT1 NLS	This work	N/A
pcDNA3.1(-)5mCitrine-STAT1 NLS M691V	This work	N/A
pcDNA3.1(-)5mCitrine-Cyclin B1 NLS	This work	N/A
pcDNA3.1(-)5mCitrine-Cyclin B1 NLS S3E	This work	N/A
pcDNA3.1(-)5mCitrine-Cyclin B1 NLS S3E M|V	This work	N/A

(*Continued on next page*)

Continued

REAGENT or RESOURCE	SOURCE	IDENTIFIER
pcDNA3.1(-)5mCitrine-CRS	This work	N/A
pcDNA3.1(-)5mCitrine-CRS S4E	This work	N/A
pcDNA3.1(-)5mCitrine-CRS S4E M|V	This work	N/A
pcDNA3.1(-)5C-FRB-KNS	This work	N/A
pcDNA3.1(-)5C-FRB-KNS M359V	This work	N/A
pcDNA3.1(-)5C-FRB-KNS neutral	This work	N/A
pcDNA3.1(-)3mCitrine-TAZ NLS M337V	This work	N/A
pcDNA3.1(-)5mCitrine-VSV-M NLS	This work	N/A
pcDNA3.1(-)5mCitrine-VSV-M NLS M|V	This work	N/A
pcDNA3.1(-)5mCitrine-KSHV-TRX1 NLS	This work	N/A
pcDNA3.1(-)5mCitrine-RVFV-NSs NLS	This work	N/A
pcDNA3.1(-)5mCitrine-RVFV-NSs NLS M|V	This work	N/A
pcDNA3.1(-)5mCitrine-CV-M NLS	This work	N/A
pcDNA3.1(-)5mCitrine-TMEV-L NLS	This work	N/A
pcDNA3.1(-)5mCitrine-TMEV-L NLS M|V	This work	N/A
pcDNA3.1(-)5mCitrine-SARS-ORF6 NLS	This work	N/A
pcDNA3.1(-)5mCitrine-SARS-ORF6 NLS M|V	This work	N/A
pcDNA3.1(-)5mCitrine-SARS2-ORF6 NLS	This work	N/A
pcDNA3.1(-)5mCitrine-SARS2-ORF6 NLS M|V	This work	N/A
pcDNA3.1(-)5mCitrine-RVFV-NSs	This work	N/A
pcDNA3.1(-)5mCitrine-RVFV-NSs M|V	This work	N/A
pcDNA3.1(-)5mCitrine-SARS2-ORF6	This work	N/A
pcDNA3.1(-)5mCitrine-SARS2-ORF6 M|V	This work	N/A
pcDNA3.1(-)mCherry-SARS2-ORF6 NLS	This work	N/A
pcDNA3.1(-)mCherr-SARS2-ORF6 NLS M|V	This work	N/A
pcDNA3.1(-)mCherry-SARS2-ORF6	This work	N/A
pcDNA3.1(-)mCherry-SARS2-ORF6 M|V	This work	N/A
pcDNA3.1(-)mCherry-RVFV-NSs	This work	N/A
pcDNA3.1(-)mCherry-VSV-M	This work	N/A
pcDNA3.1(-)mCherry-VSV-M M|V	This work	N/A
pcDNA3.1(-)mCherry-SV40 NLS	This work	N/A
pcDNA3.1(-)mCherry-TAZ 4SA	This work	N/A
pcDNA3.1(-)mCherry-TAZ 4SA ΔNLS	This work	N/A
pcDNA3.1(-)mCitrine-RAE1	This work	N/A
pcDNA3.1(-)5mCitrine-MRTF(B)	This work	N/A
pcDNA3.1(-)5mCitrine-MRTF(B) N-term	This work	N/A
pcDNA3.1(-)mCitrine-p65 (191-300)	This work	N/A
pcDNA3.1(-)mCitrine-p65 (191-308)	This work	N/A
pcDNA3.1(-)myc-mCherry	This work	N/A
pcDNA3.1(-)myc-mCherry-TAZ	This work	N/A
pcDNA3.1(-)myc-mCherry-TAZ NLS	This work	N/A
Software and algorithms		
Metamorph premier Image analysis software	Molecular devices	https://www.moleculardevices.com/products/cellular-imaging-systems/acquisition-and-analysis-software/metamorph-microscopy#gref
Fiji	ImageJ	https://imagej.net/Fiji
Prism software version 10.3.0	GraphPad	https://www.graphpad.com/scientific-software/prism/

(*Continued on next page*)

Continued

REAGENT or RESOURCE	SOURCE	IDENTIFIER
CellProfiler software	Broad Institute	https://cellprofiler.org/
Slimsearch4	SLiMTeam - Davey lab[119]	https://slim.icr.ac.uk/tools/slimsearch/input?motif=
Cytation 5 system	BioTek, Agilent	https://www.agilent.com/en/product/cell-analysis/cell-imaging-microscopy/cell-imaging-multimode-readers/biotek-cytation-5-cell-imaging-multimode-reader-1623202
ImageXpress Micro system	Molecular devices	https://www.moleculardevices.com/products/additional-products/imagexpress-micro-xls-widefield-high-content-analysis-system
Image Lab Software 6.1.0	Bio Rad	https://www.bio-rad.com/en-ca/product/image-lab-software?ID=KRE6P5E8Z
Image Studio 6.0	LI-COR BIOTECH	https://www.licorbio.com/image-studio

EXPERIMENTAL MODEL AND STUDY PARTICIPANT DETAILS

Cells

Tissue culture media and reagents were from Thermo Fisher/Life Technologies. Culture media was supplemented with 10% fetal bovine serum and 1% penicillin/streptomycin, and cells were grown in a humidified atmosphere containing 5% CO2.

LLC-PK1, a kidney tubule epithelial cell line (male) was a gift from R.C. Harris, Vanderbilt University School of Medicine and was cultured in low-glucose DMEM as described in.[58] HEK (HEK293T Cat# CRL-3216, RRID:CVCL_0063), a human epithelial-like embryonic kidney cell line (female) was a gift from Gagan Gupta (Toronto Metropolitan University). These cells were cultured in high-glucose DMEM. hTERT RPE cells, a Telomerase immortalized human retina pigmented epithelial cell line (female) were obtained from the American Type Culture Collection (ATCC Cat# CRL-4000, RRID:CVCL_4388). RPE cells were cultured in DMEM-F12. Where indicated, cells were treated with LMB (20 ng/ml), Rapamycin (1 nM), TNFα (20 ng/ml) or ivermectin (25 μM, or with indicated concentrations) for varying times depending on the experimental procedure. Cell contact disassembly was achieved by thoroughly washing cultures in PBS and placing them in nominally calcium chloride-free DMEM (low calcium medium, LCM). Antiviral signaling pathways were triggered by transfecting cells with poly(I:C) (100 ng/ml) using jetPrime (PolyPlus Transfection SA) according to the manufacturer's instructions. For ATP-depletion, cells were incubated in DMEM without glucose, supplemented with 1 g/l 2-deoxyglucose and 10 mM sodium azide. Cells were regularly tested for mycoplasma contamination.

METHOD DETAILS

Reagents

Leptomycin B, Rapamycin, Ivermectin, and poly(I:C) were purchased from Sigma-Aldrich. TNFα is from Abcam.

Antibodies

For western blot analysis, proteins were detected using the following antibodies from Santa Cruz Biotechnology: anti-GFP (SC-8334, 1:1000), anti-IPO7 (SC-365231, 1:250), anti-KPNA2 (SC-55538, 1:500), anti-KPNB1 (SC-137016, 1:500), anti-RAE1 (SC-393252, 1:500), and anti-DsRed (SC-390909, 1:1000). Cell Signaling Technology was the source for anti-GFP (#2555S, 1:1000), anti-tubulin (#2128S, 1:1000), and anti-YAP/TAZ (#8418S, 1:1000). The anti-c-Myc antibody was purchased from Thermo Fisher Scientific, A1HO0062, 1:1000). Jackson ImmunoResearch Laboratories was the source for all horseradish peroxidase-conjugated secondary antibodies (1:5,000). Mandel Scientific was the source for IRDye680RD and IRDye800CW conjugated secondary antibodies (1:5000). For immunofluorescence staining, proteins were detected using the following antibodies from Cell Signaling Technology: anti-IRF3 (#4302S, 1:100), anti-YAP/TAZ (#8418S, 1:100) and anti-MRTF (#97109S, 1:100). Anti-p65 (SC-8008, 1:50) was from Santa Cruz Biotechnology and anti-TAZ (560235, 1:100) from BD Biosciences. Alexa 488 or 555 conjugated secondary antibodies were from Thermo Fisher Scientific (1:500).

Plasmid and small-interfering RNA (siRNA) transfection

The myc-tag expression vector with AscI and PacI sites, pcDNA3.1(-)mCherry, pcDNA3.1(-)mCitrine, pcDNA3.1(-)3mCitrine, pcDNA3.1(-)5mCitrine, pcDNA3.1(-)mCitrine-TAZ 4SA, pcDNA3.1(-)5mCitrine-TAZ 4SA, pcDNA3.1(-)5mCitrine-TAZ (327-341 = NLS), pcDNA3.1(-)5mCitrine-R5A and pcDNA3.1(-)5mCitrine SV40 NLS were described previously.[32] YAP 5SA was a gift from Jeff Wrana.[118] MRTF fragments and mutants were described previously.[7] The coding sequence for RVFV-NSs was obtained from

Sino Biological (VG40339-G). The following constructs were obtained from Addgene and gifts of the mentioned researchers: IKK-2 S177E S181E (Anjana Rao; #11105),[101] pcDNA-GFP-STAT1 (Steven Johnson; #11987), pCAG-VSVM (Ian Wickersham; #64086), and GFP-RelA (Warner Greene; #23255).[120] INFβ promoter-luciferase reporter (pGL3-INFβ-luc) was a gift from Drs John Hiscott of McGill University and Marc Servant of Université de Montréal, QC, Canada). NFkB promoter-luciferase reporter (pGL4.32[luc2P/NF-κB-RE/Hygro]) and pRL-TK was from Promega.

Coding sequences for TAZ, YAP, p65, VSV-M, RVFV-NSs, and MRTF were amplified from templates using standard PCR techniques. For SARS, SARS2, KNS and CRS, coding sequences were assembled from overlapping oligonucleotides. Oligonucleotide DNA duplexes were utilized to produce shorter inserts encoding the various NLS versions or the Rev NES (aa71-84) in pcDNA3.1(-)5mCitrine-R5A-NES. DNA fragments were inserted into pcDNA3.1(-)mCherry, pcDNA3.1(-)mCitrine, pcDNA3.1(-)3mCitrine, pcDNA3.1(-)5mCitrine or pcDNA3.1(-)5mCitrine-R5A using AscI and PacI sites. Point mutations, deletions and insertions were created by standard overlapping PCR techniques. For myc-mCherry expression, mCherry-fusion coding regions were amplified with primers adding MluI and PacI restriction sites at the 5′- and 3′-end, respectively. These restriction sites were used to insert the DNA fragments into the myc-tag expression vector, cleaved with AscI and PacI. For all PCR reactions a high-fidelity proof-reading polymerase (Phusion; Thermo Scientific) was used. Restriction enzymes were purchased from New England BioLabs. All constructs generated were verified by sequencing. Transfections were performed using jetPrime (PolyPlus Transfection SA) or Polyjet (SignaGen Laboratories PolyJet) according to the manufacturer's instructions. Porcine-specific siRNAs used in knockdown experiments were directed against the following sequences: TAZ 5′-CAAGAACATACACCTACGGTTGT-3′; YAP 5′-TCAAAGCGCTC CAGTGAAA-3′; RAE1 5′- GGACAAAGATGCCAGAACA-3′; RAN 5′-GCAACAAAGTGGATATTAA-3′. Oligonucleotides were synthesized and purchased from Thermo Scientific or Sigma-Aldrich. NR control siRNA was obtained from Applied Biosystems. Cells were transfected with 100 nM siRNAs alone or together with plasmids using jetPRIME and were analysed for silencing or the cellular localisation of co-transfected constructs 48h later.

Luciferase reporter assay

Cells were transfected with pGL3-INFβ-luc or pGL4.32[luc2P/NF-κB-RE/Hygro], the normalizing plasmid pRL-TK (Promega) and mCherry constructs. Renilla luciferase and firefly luciferase activities in cell lysates were measured using a reporter assay system (Dual Luciferase; Promega) in a BioTek Synergy Microplate Reader (Agilent). Firefly/renilla ratios are expressed as fold changes compared to the firefly/renilla ratio of the untreated control.

Immunoprecipitation and Western blotting

Immunoprecipitations were done using transiently transfected HEK or untransfected LLC-PK1 cells, grown in 10 cm dishes. Cells were lysed in lysis buffer (20 mM Hepes, pH 7.5, 137 mM NaCl, 3 mM KCl, 1 mM EDTA, 1 mM EGTA, 10% glycerol and 0.5% NP-40) supplemented with 1 mM PMSF, 1 mM Sodium Vanadate and Complete Mini Protease Inhibitor (Roche). Lysates were spun at 4°C, 12,000 rpm for 2 min to remove cell debris and analyzed for protein content (BCA Protein Assay; Pierce Biotechnology). Supernatants were precleared with protein A/G beads (Pierce) for 1h, incubated with GFP-trap beads (ChromoTek) for 1h or antibodies overnight following 1h incubation with protein A/G beads. Beads were washed three times with washing buffer (lysis buffer containing 0.05% NP-40). Bound proteins were eluted using SDS-PAGE sample buffer. Inputs and eluted proteins were subjected to SDS-PAGE followed by Western blot analysis using nitrocellulose membranes. Immunodetections were either performed using HRP-coupled secondary antibodies and ECL Plus reagents (GE Healthcare, Life Sciences) with a BioRad Chemidoc Imager or fluorescent secondary antibodies and the infrared Odyssey imager (LI-COR). Images were processed and quantified using the platform-specific BioRad Image Lab Software and LI-COR Image Studio suits, respectively. All quantified experiments were performed a minimum of three times and representative immunoblots are shown.

Immunofluorescence microscopy

For immunofluorescence microscopy, LLC-PK1 cells were grown on glass coverslips or 96 well plates (Corning), transfected with constructs and/or siRNA for 24-48h and fixed with 4% paraformaldehyde. Following permeabilization with 0.1% Triton X-100 and blocking with BSA, cells were first incubated with primary antibody and then with fluorescently conjugated secondary antibody and DAPI (Lonza). For fluorescence microscopy, cells were transfected with constructs for 24h, fixed with 4% paraformaldehyde and incubated with DAPI. Coverslips were mounted on slides using fluorescent mounting medium (Dako). Images were captured using a WaveFX spinning-disk microscopy system (Quorum Technologies, Guelph, Canada) equipped with ORCA-Flash4.0 digital camera, driven by the MetaMorph software and analysed using the CellProfiler software (Broad Institute).[121] 96 well plates were imaged using the ImageXpress Micro system (Molecular Devices) or the Cytation 5 system (BioTek, Agilent) and analysed with the inbuilt analysis routines. All nuclear-to-cytoplasmic fluorescence ratios (N/C) were computed based on nuclear and cytoplasmic compartment masks, derived from DAPI images, as described previously.[32,56] Briefly, the nuclear compartment mask for each cell was calculated by shrinking the automatically detected nucleus mask from DAPI-images. A ring around the nuclear mask represents the corresponding cytoplasmic compartment mask. Large numbers of cells (>100-5000) were used to calculate individual median N/C values. All image processing was done according to the Journal's guidelines.

FRAP experiments

For import studies, LLC-PK1 cells plated into 35-mm glass bottom dishes (MaTek) were transfected with 3C-constructs. Experiments were performed 24 h later. Cells were placed in a TC-L-10 live incubation device and live images were taken using the WaveFX spinning-disk microscopy system and an ILas2 FRAP module. The following imaging settings were used: twenty images at 1 sec intervals, ten at 5 sec intervals, ten at 10 sec intervals and twenty at 30 sec intervals. Bleaching of the nuclear region of interest with a 488-nm laser (bleach) occurred after the first nine images. Data were collected from the bleached compartment (nucleus), the non-bleached compartment (cytoplasm) within the same cell and a non-bleached control region outside of the cell of interest for background correction. N/C values were plotted against acquisition times and recovery curves were fitted to a mono-exponential function, excluding early time points (<15 sec) where intranuclear diffusion convolutes fluorescence recovery by import.

M-motif search

The search for publications describing proteins with TAZ NLS-like nuclear import modalities (e.g. unconventional NLS, Ran/ATP-independent import) lead to the identification of cyclin B1, STAT1 and hnRNPK. Sequences were then manually inspected for the presence of a methionine with flanking negative charges. In cyclin B1, such a motif was found in the CRS, phosphorylation of two serines in the vicinity of the methionine provided the flanking negative charges and these posttranslational modifications were implicated in the regulation of the nuclear localization of cyclin B1[77,105,106]. Similarly, STAT1 compromised an easily identifiable motif centered around M691. In case of hnRNPK, while the KNS did not comprise a such a motif, methionines and multiple negative charges are clustered, suggesting the presence of a functional motif based on strong compositional similarity. Sequence similarity between TAZ M-motif and the reported viral proteins was also manually affirmed. Combining the mutational analysis of the TAZ NLS with functional M-motifs in STAT1, cyclin B1 and viral proteins, we deduced the consensus motif (-)x<1,2>M(-)[TILVMWFY]x<0,1>(-), were (-) represents negatively charged or phosphorylated residues, x <a,b> any residue occurring a-b times. This motif, excluding instances with phosphorylated residues, was found in 473 human and 256 viral proteins, using the webpage Slimsearch4.[119]

QUANTIFICATION AND STATISTICAL ANALYSIS

Data are presented as blots or images from at least three similar experiments. For the calculation of individual median N/C data points, more than 100-5000 transfected cells were analysed for each condition. Data are presented as scatter plots with mean ± standard deviation (SD), as indicated. The number of experiments (n) analyzed is shown on the graphs above the data sets or reported in the figure legends. Statistical significance was determined by one-way analysis of variance (ANOVA, Tukey posthoc testing) for comparison of multiple groups. For normalized values (Figures 5J, S8B, and S8E), we utilized a one sample t-test. $p < 0.05$ was accepted as significant; *, **, and *** correspond to $p < 0.05$, <0.01, and <0.001, respectively. Statistical analysis and curve fitting was performed using the GraphPad Prism software (version 10, GraphPad Software Inc.).